EXPERIMENTAL-THEORETICAL STUDY OF VELOCITY FEEDBACK DAMPING OF STRUCTURAL VIBRATIONS

by

Gary R. Skidmore

Dissertation submitted to the Faculty of the
Virginia Polytechnic Institute and State University
in partial fulfillment of the requirements for the degree of
Doctor of Philosophy
in
Aerospace Engineering

APPROVED:

William L. Hallauer, Jr.

Frederick H. Lutze

Karl Sundkvist

Eugene M. Cliff

Scott L. Hendricks

May, 1985

Blacksburg, Virginia

EXPERIMENTAL-THEORETICAL STUDY OF VELOCITY FEEDBACK DAMPING OF STRUCTURAL VIBRATIONS

by

Gary R. Skidmore

(ABSTRACT)

This study concerns the active damping of structural vibrations through the application of various forms of velocity feedback control. Active damping will be required for large space structures which are performance-sensitive to motion or inaccurate pointing. Several control forms, including modal-space active damping and direct rate feedback, are analyzed theoretically, and three laboratory models are described. A previous, unsuccessful attempt at control is reviewed and explained. The remaining control forms developed in the theoretical section were implemented successfully and the results compare favorably with theoretical predictions. Each control form is analyzed relative to its own merits and in comparison with other methods. An important point is the stability assured by a dual (colocated) configuration of velocity sensors and control force actuators. Modal-space active damping is shown to be an effective control method with predictable performance in controlled modes and beneficial spillover into residual (non-controlled) modes.

ACKNOWLEDGEMENTS

I am greatly indebted to Dr. William Hallauer Jr., my advisor, for his patience, guidance, and assistance throughout the course of my graduate work. The original ideas for the laboratory models and much of the intended research were his. His keen insight and attention to detail helped to solve many problems encountered during the research.

I would like to thank the members of my committee; Dr. Fred Lutze, Dr. Gene Cliff, Dr. Karl Sundkvist, and Dr. Scott Hendricks.

I extend my gratitude to Dr. Anthony Amos and the Air Force Office of Scientific Research for the financial support of this research under Grant AFOSR-82-0217 and Contracts F49620-83-C-0158 and F49620-85-C-0024.

I also extend my gratitude to the National Science Foundation for NSF Grant number CME-8014059, which funded the purchase of the data acquisition equipment used in the experimental part of this research.

I am extremely grateful for the endowment provided by George and Gladys Cunningham making possible the Cunningham Dissertation Year Fellowship which I was fortunate to receive.

I am grateful for the friendship, support, and assistance of my fellow graduate students through the years, particularly

and

provided a great deal of technical assistance in the laboratory, and his help was deeply appreciated.

I would like to thank my extremely patient wife, , for her constant support and encouragement; and I would also like to

express my appreciation to her family, for all of their help and kindness.

TABLE OF CONTENTS

LIST OF ILLUSTRATIONS

LIST OF TABLES

1.0 INTRODUCTION

This study pertains to the active damping of structural vibrations. The intended application is for a large space structure (LSS) which is being disturbed by environmental or maneuver actions or is vibrating freely following such excitation. Large flexible spacecraft or other space structures will require active damping (control) to augment low inherent damping and maintain the integrity of overall system performance, which may depend on pointing accuracy or a desired static shape, for instance.

In general, active damping would be supplied by feedback from an array of distributed sensors, acting through a control law, driving an array of distributed actuators. This control could evolve from any of several basic philosophies. Simple rate or position feedback control, modal control, and optimal (modern) control are three examples of philosophies of control. Rate, or velocity, feedback consists essentially of attaching one or more physical dashpots to the structure in question to dissipate vibrational energy. What is referred to as modal control (with velocity feedback) is a means of applying a "modal dashpot" to the structure by working through the decoupled modal equations of motion. Modern or optimal control generally refers to controller design which minimizes some performance index consisting of structural states and control forces.

A great number of studies of active vibration control of large space structures have been produced in the past several years. The quantity of work which has been reported places an extensive literature review

beyond the scope of this dissertation. In fact, Reference 1 is devoted entirely to just such a survey and cites nearly 200 studies. A vast majority of published studies have concentrated solely on theoretical work; of the citations in Reference 1, only 13 are experimental in nature. Of this relative minority of experimental efforts, very few have presented comparisons of experimental and theoretical results. Such experimental-theoretical correlations are necessary in order to fully evaluate the performance of a control concept before it can be applied. These comparisons also would help to explain what makes some concepts successful or causes others to fail.

References 2-5 are representative of the most significant experimental studies. Aubrun et al[2] implemented a form of optimal control using modal states rather than physical states. The authors placed an emphasis on hardware mechanization of control and an important aspect of their work is the use of structure-borne sensors and actuators. Reference 2 is rare in that it forthrightly discusses some of the typical problems encountered in experimental work, and in the quality of data presentation. The authors also include a tabulation of several LSS experiments conducted by various researchers. Schaechter and Eldred[3] describe the construction of a flexible beam laboratory structure and the implementation of various control forms, including both shape and motion control, using optimal and adaptive control strategies. Bauldry et al[4] have implemented optimal estimation and control algorithms on perhaps the most challenging structure to date, a three dimensional flexible offset-feed antenna. The study used entirely structure-borne actuators and sensors, which not many have done. Meirovitch et al[5] describe an

experimental implementation of a form of modal control on a beam structure, using a nonlinear control method with quantized forces supplied by externally supported, contacting actuators. While References 3 through 5 represent significant experimental implementations of active structural control, they are also representative of the relatively uninformative experimental data which has been published, consisting primarily of time histories of response with no theoretical correlation.

In the present study, several forms of active damping were applied to laboratory models using velocity feedback between noncontacting, externally supported velocity sensors and force actuators. The primary objectives were successful implementation, gathering of extensive experimental data, and correlation with theory. Structure-borne hardware was not employed, as this study was concerned primarily with validation of theoretical control concepts, and because there was no funding for such hardware.

The theoretical development of each control form applied in this study is presented in Chapter 2. The theory contained therein consists of independent, natural derivations of control strategies, although the various forms can be traced to several previous authors. Chapter 3 gives a brief description of the laboratory models which were employed, and Chapter 4 presents the equipment used for control implementation, experimental testing, and data acquisition. Experimental results and comparisons with theory are discussed in separate chapters, each describing the implementation of a different form of control. Chapter 5 reviews and connects previous work[6,7,8] which attempted modal active damping involving dynamic compensation in the form of frequency filters.

A revised form of modal active damping requiring no dynamic compensation was implemented and is discussed in Chapter 6. This method can be shown to be identical to the method of Canavin.[9] The importance of actuator-sensor colocation is also discussed in Chapter 6. Chapter 7 presents results for an optimized form of direct velocity feedback active damping using multiple actuator-sensor pairs. Chapter 8 discusses an attempt to extend modal active damping to control of a greater number of modes than actuators as in Elliot et al.[10] In Chapter 9, results for a combination of modal control and rate feedback are presented. A summary and conclusions are given in Chapter 10.

2.0 THEORETICAL ANALYSIS OF CONTROL SYSTEMS

The control methods used in this study involved various forms of linear rate feedback. Velocity sensors were used to measure velocity at one or more points (degrees of freedom) on the structure, and the resulting velocity signals were multiplied by gain factors and fed back to force actuators to provide active viscous damping.

In order to model the closed-loop system, one begins with an N-DOF discretization of the structure and forms the N equations of motion given by

$$[m]\{\ddot{q}\} + [d]\{\dot{q}\} + [k]\{q\} = \{f^c\} + \{f^e\}, \tag{1}$$

where [m], [d], and [k] represent mass, inherent damping, and stiffness matrices; {q} is the vector of grid point displacements; $\{f^e\}$ is the excitation (or disturbance) vector; and $\{f^c\}$ is the vector of control actions. The structural damping is approximated with noncoupling modal viscous damping. It is assumed that the first n normal modes of vibration are known or can be calculated, so that one can use a truncation of the standard modal transformation, $\{q\}=[\Phi]\{\xi^n\}$, with modal matrix $[\Phi]$ and n modal coordinates $\{\xi^n\}$. Applying standard orthogonality conditions gives the equations of motion in modal coordinates as:

$$[M]\{\ddot{\xi}^n\} + [D]\{\dot{\xi}^n\} + [K]\{\xi^n\} = [\Phi]^T(\{f^e\} + \{f^c\}) \tag{2}$$

where the modal mass, inherent damping and stiffness matrices are given by

$$[M] = [\Phi]^T[m][\Phi] = \text{diag}(M_r,\ r=1,2,\ldots,n),$$
$$[D] = \text{diag}(2M_r\omega_r\zeta_r,\ r=1,2,\ldots,n), \text{ and}$$
$$[K] = \text{diag}(M_r\omega_r^2,\ r=1,2,\ldots,n)$$

where ω_r and ζ_r denote the natural frequency and viscous damping factor of the r^{th} mode.

The control force vector, $\{f^c\}$, can be expressed in the form of rate feedback control as $\{f^c\}=\{c(\{\dot{q}^s\})\}$; a vector-valued function of the vector of physical velocities. The only nonzero terms of the forcing vector are the n_a terms relating to the degrees of freedom where actuators are located, so that $[\Phi]^T\{f^c\} = [\Phi^a]^T\{c^a\}$, where $[\Phi^a]$ contains only the rows of $[\Phi]$ corresponding to actuator locations and $\{c^a\}$ is an n_a-element vector. Equation 2 with this substitution becomes

$$[M]\{\ddot{\xi}^n\} + [D]\{\dot{\xi}^n\} + [K]\{\xi^n\} = [\Phi^a]^T\{c^a(\{\dot{q}^s\})\} + [\Phi]^T\{f^e\}. \qquad (3)$$

2.1 MODAL-SPACE ACTIVE DAMPING

The basic concept of modal-space control, in the context of active viscous damping, is that the feedback term is a function of modal velocities, rather than physical velocities. Ideally, the control would be uncoupled in the modal space, in order to damp individual target modes independently. Since only the physical velocities (at a finite number

of locations, n_s) can actually be measured, some manner of estimation must be used to obtain the modal velocities from the set of measured physical velocities, $\{\dot{q}^s\}$. Once this is accomplished, the modal-space control force vector can be written as a function of the modal velocities of the modes to be controlled;

$$[\Phi]^T\{f^c\} = [\Phi^a]^T\{c^a(\{\dot{\xi}^c\})\}.$$

Two different methods of obtaining estimates of modal velocities were used in this research. The first employed only one velocity sensor and relied on spectral filtering to discern modal content. The second used an array of sensors and a spatial filter based on presumed knowledge of the vibration mode shapes. Spectral filtering refers to filtering based on signal frequency content, and thus works over certain ranges of the frequency spectrum, whereas spatial filtering is based on relative responses from a number of spatially distributed sensors.

2.2 SPECTRAL FILTERING

The modal estimator for the case of spectral filtering consisted of a single velocity sensor and a number of narrow-band band-pass filters. The output of a velocity sensor in DOF i contains contributions from all n modes in the model as given by

$$\dot{q}_i = \sum_{j=1}^{n} \phi_{ij}\dot{\xi}_j. \qquad (4)$$

For each controlled mode, the passband of a spectral filter was centered on that mode's natural frequency. In this way, only that part of the measured response, $\dot{q}_i$, which occurred at the frequency of the controlled mode would be transmitted to the controller. An ideal filter, acting on the transient response of a structure with no damping, would pass only the response of the controlled mode. However, each mode of a real structure with nonzero damping responds at all frequencies. Using band-pass filters simply ignores the off-resonant response of each mode. In other words, the actual output of a spectral filter contains not only the resonance of the corresponding controlled mode, but also some of the off-resonant response of every other mode. Additionally, the filter actually excludes some of the response of the controlled mode, that which lies outside the passband. These effects were neglected in order to facilitate the calculation of control gains. With the sensor output, $\dot{q}_i$, directed through parallel spectral filters, it was assumed that the output of the filter for mode s was proportional to the modal velocity of mode s:

$$\hat{y}_s = \phi_{is}\dot{\xi}^c_s \quad (\text{s over controlled modes}).$$

With this assumption, the control force vector could be expressed as

$$\{c^a\} = [C^{ac}]\{\hat{y}\} = [C^{ac}][\Phi^c_i]\{\dot{\xi}^c\},$$

where $[C^{ac}]$ is the active control matrix (yet to be determined), $\{\hat{y}\}$ is the vector of ideal filter outputs, and $[\Phi^c_i] = \text{diag}(\phi_{is}$, s over

controlled modes). The equations of motion for only the controlled modes then becomes

$$[M^c]\{\ddot{\xi}^c\} + [D^c]\{\dot{\xi}^c\} + [K^c]\{\xi^c\} = [\Phi^{ac}]^T [C^{ac}][\Phi_i^c]\{\dot{\xi}^c\}, \qquad (5)$$

where superscript c denotes appropriate partitions for the controlled modes, and the disturbance vector, $\{f^e\}$, has been omitted.

In this research, control was desired in the form of active modal viscous damping, so that the required form of Equation 5 was

$$[M^c]\{\ddot{\xi}^c\} + [D^c]\{\dot{\xi}^c\} + [K^c]\{\xi^c\} = -[D^A]\{\dot{\xi}^c\}, \qquad (6)$$

where the active damping matrix is given by

$$[D^A] = \text{diag } (2M_s\zeta_s^c\omega_s, \text{ s over controlled modes}),$$

which is an additive generalized damping term with specified viscous damping factors ζ_s^c (here, superscript A is used to imply "active", whereas superscipt a is used to denote partitions relative to actuator locations). Inspection of Equation 5 and Equation 6 yields a solution for the control matrix, $[C^{ac}]$, which would preserve uncoupled controlled modes in the ideal case:

$$[C^{ac}] = -[\Phi^{ac}]^{-T} [D^A][\Phi_i^c]^{-1} \qquad (7)$$

(provided that the indicated inverses exist). The assumption involved in Equation 5 must now be relaxed in order to accurately model the system, for which the actual feedback term is

$$\{c^a\} = [C^{ac}]\{y\},$$

where $\{y\}$ is the vector of actual filter outputs. The full set of n dynamic equations then becomes

$$[M]\{\ddot{\xi}^n\} + [D]\{\dot{\xi}^n\} + [K]\{\xi^n\} = [\Phi^a]^T [C^{ac}]\{y\}. \tag{8}$$

The band-pass filters used in this research were designed by Forward[11] and were described in detail by Skidmore.[6] The dynamics of these filters (or of any other filters) must be accounted for, as has been done in References 7 and 8. The equation describing filter s (for mode s) is

$$\ddot{y}_s + B_s\dot{y}_s + \omega_{cs}^2 y_s = B_s\ddot{q}_i, \tag{9}$$

in which $\dot{q}_i$ is the input signal, y_s is the filter output, B_s is the filter half-power bandwidth, and ω_{cs} is the center frequency of the passband, equal to the frequency of mode s. Also, the input to the filters, $\dot{q}_i$, can be expressed as in Equation 4. With these substitutions, the total system is described by a set of structural equations coupled together with a set of filter equations:

$$[M]\{\ddot{\xi}^n\} + [D]\{\dot{\xi}^n\} + [K]\{\xi^n\} - [\Phi^a]^T[C^{ac}]\{y\} = [\Phi]^T\{f^e\} \qquad (10)$$

and

$$[I]\{\ddot{y}\} + [B]\{\dot{y}\} + [\omega_c^2]\{y\} - [B][T_s][\Phi]\{\ddot{\xi}^n\} = \{0\}. \qquad (11)$$

In Equation 11, [I] is an identity matrix of order n_c; [B]=diag(B_s, s over n_c); $[\omega_c^2]$= diag(ω_{cs}^2, s over n_c); $[T_s]$ is a transformation matrix relating $\dot{q}_i$ to $\{\dot{q}\}$ (n_c by N); and $[C^{ac}]$ has the form prescribed by Equation 7.

At this point, a new state vector comprised of $\{\xi\}$ and $\{y\}$ can be used to permit closed-loop frequency response analysis and eigensolution in the state-space, as was detailed in References 7 and 8.

Potential hazards involved in employing spectral filtering arise from the fact that all modes of a structure respond to all forcing frequencies (a filter centered on the resonance of one mode will pass some contributions from each and every mode), and from possible dynamic coupling between the filters and the structure.

2.3 SPATIAL FILTERING

An alternative to spectral filtering in the estimation of modal response is to use more sensors and employ a priori knowledge of the structure's mode shapes to discern modal content. This is the essence of a spatial filter. The availability of a number of sensors (n_s) permits Equation 4 to be expanded to

$$\{\dot{q}^s\} = [\Phi^s]\{\dot{\xi}^n\}, \tag{12}$$

where $[\Phi^s]$ contains rows of $[\Phi]$ corresponding to the n_s sensor locations. Since a matrix inversion would be necessary in order to solve directly for modal response given a set of physical responses, $[\Phi^s]$ must be square, at least in the strictest definition of an inverse. This dictates that the number of sensed modes, n_m, must equal the number of sensors, n_s. This leads to an equation of the form

$$\{\dot{q}^s\} = [\Phi^{rs}]\{\dot{\xi}^s\}, \tag{13}$$

where $[\Phi^{rs}]$ is a square, reduced form of $[\Phi^s]$. However, this is based on the assumption that only n_s modes contribute significantly to the total structural response. With this assumption, the estimated modal response is given simply by

$$\{\dot{\xi}^s\}^* = [\Phi^{rs}]^{-1}\{\dot{q}^s\}, \tag{14}$$

where the superscript * indicates an estimate to the true value. This estimation approach has been referred to by others as static observation[2,9] and modal filtering.[12]

Using Equation 13 for the controller input creates a control force vector of the form

$$\{c^a\} = [C^{ac}][\Phi^{rs}]\{\dot{\xi}^s\},$$

where $[C^{ac}]$ will have to be redefined. Equation 3 then becomes

$$[M]\{\ddot{\xi}^n\} + [D]\{\dot{\xi}^n\} + [K]\{\xi^n\} = [\Phi^a]^T [C^{ac}][\Phi^{rs}]\{\dot{\xi}^s\} \tag{15}$$

where the disturbance vector has been omitted.

The desired form of the control term for modal-space active damping is given by

$$[\Phi^{ac}]^T [C^{ac}][\Phi^{rs}]\{\dot{\xi}^s\} = -[D^A]\{\dot{\xi}^c\}. \tag{16}$$

The first step in the solution of Equation 16 is to allow

$$[C^{ac}] = [\Phi^{ac}]^{-T} [C_1][\Phi^{rs}]^{-1}$$

(provided the indicated inverses exist, hence the requirement that $[\Phi^{rs}]$ be square), so that Equation 16 becomes

$$[\Phi^{ac}]^T [C^{ac}][\Phi^{rs}]\{\dot{\xi}^s\} = [C_1]\{\dot{\xi}^s\}, \tag{17}$$

where $[C_1]$ is an n_c by n_s matrix (in general, non-square). To allow for the potential case of controlling fewer modes than the number of sensed modes ($n_c < n_s$), $[C_1]$ must be a product of the matrix $-[D^A]$ and a transformation matrix $[T_s]$ which eliminates modes that are sensed but not controlled:

$$[C_1] = -[D^A][T_s],$$

where $[T_s]$ is a null matrix, except for ones in the locations relating each of the controlled modes to its corresponding sensed mode. The control matrix is thus defined by

$$[C^{ac}] = -[\Phi^{ac}]^{-T}[D^{A}][T_s][\Phi^{rs}]^{-1}, \tag{18}$$

where $[D^{A}]$ retains the original meaning.

The assumption made in Equation 13, which permitted a simple solution for the control matrix, Equation 18, must now be relaxed. That is, an accounting must be made of the fact that the structure responds to some extent in all modes, not just those that are sensed. Equation 12 is thus used to obtain the final form of the system equation:

$$[M]\{\ddot{\xi}^{n}\} + [D]\{\dot{\xi}^{n}\} + [K]\{\xi^{n}\} = [\Phi^{a}]^{T}[C^{ac}][\Phi^{s}]\{\dot{\xi}^{n}\}. \tag{19}$$

This formulation allows for the prediction of error in the modal estimation process. This error can be derived through manipulation of Equation 12 and Equation 13 if one partitions $[\Phi^{s}]$ as

$$\{\dot{q}^{s}\} = [\Phi^{rs}]\{\dot{\xi}^{s}\} + [\Phi^{us}]\{\dot{\xi}^{u}\}, \tag{20}$$

where $\{\dot{\xi}^{u}\}$ and $[\Phi^{us}]$ relate to unretained modes (or more specifically, unobserved modes). The presumed modal estimate is given by Equation 14, so pre-multiplication of Equation 20 by $[\Phi^{rs}]^{-1}$ gives

$$\{\dot{\xi}^{s}\}^{*} = [\Phi^{rs}]^{-1}\{\dot{q}^{s}\} = \{\dot{\xi}^{s}\} + [\Phi^{rs}]^{-1}[\Phi^{us}]\{\dot{\xi}^{u}\}. \tag{21}$$

So the modal estimation error, which is included in the theoretical model and present physically, is given by

$$(\{\dot{\xi}^s\}^* - \{\dot{\xi}^s\}) = \{\dot{\xi}^e\} = [\Phi^{rs}]^{-1}[\Phi^{us}]\{\dot{\xi}^u\}.$$

At this point, it is appropriate to examine a very special case of a control configuration, one with dual sensor-actuator locations. A sensor is said to be "dual"[13] with an actuator if the two are colocated and coaxial, that is, acting in the same degree of freedom. A control configuration is a dual configuration if each and every sensor is dual with an actuator.

To make modal-space active damping conform to this concept of duality, the number of sensors must equal the number of actuators, and the set of sensed modes must be the same as the set of controlled modes. This requirement leads to $[\Phi^{ac}] = [\Phi^{rs}]$ and $[T_s] = [I]$ (an n_s -order identity matrix). Thus, Equation 18 becomes

$$[C^{ac}] = -[\Phi^{ac}]^{-T}[D^A][\Phi^{ac}]^{-1}. \tag{22}$$

This result shows that $[C^{ac}]$ will always be a negative definite, symmetric matrix when dual sensor-actuator pairs are employed and $[D^A]$ is positive definite (which it always is). The importance of the negative-definiteness of $[C^{ac}]$ can be seen more clearly when it is taken to the left-hand side of the equation, as in:

$$[M]\{\ddot{\xi}^n\} + ([D]-[\Phi^a]^T[C^{ac}][\Phi^s])\{\dot{\xi}^n\} + [K]\{\xi^n\} = [\Phi]^T\{f^e\}. \tag{23}$$

Since duality also forces $[\Phi^a] = [\Phi^s]$, a negative definite $[C^{ac}]$ always results in a positive definite augmented damping matrix,

$$[AD]=([D] - [\Phi^a]^T [C^{ac}][\Phi^a]), \tag{24}$$

which guarantees system stability. Therefore, it is possible to conclude that a dual configuration of sensors and actuators will always produce a stable structure-control system.

Such an argument cannot be made for the case of control with non-dual sensors and actuators, as the quadratic forms in Equation 22 and Equation 24 do not arise.

Although the derivation and stability conclusions presented here resulted from independent analysis, Canavin[9] presented an equivalent derivation and drew the same conclusion regarding stability of a dual control configuration.

2.4 OPTIMIZED DIRECT RATE FEEDBACK DAMPING

Perhaps the simplest form of velocity feedback control is direct rate feedback damping, which is analogous to attaching one or more viscous dashpots to the structure. Direct rate feedback naturally leads to a dual configuration of the control system, with no coupling terms between non-dual sensors and actuators. Each sensor sends a feedback signal only to its dual actuator, so that the vector of control actions is simply

$$\{c^a\} = -[DF]\{\dot{q}^s\} \tag{25}$$

where $\{\dot{q}^s\}$ is the n_s-element vector of measured physical velocities; $\{c^a\}$ is an n_s-element submatrix of $\{f^c\}$; and $[DF] = \text{diag}(d_i,\ i \text{ over } n_s)$. In this form, [DF] is simply the physical active viscous damping matrix associated with the n_s ($= n_a$) physical DOFs where the dual sensor-actuator pairs are located. Since this matrix is always positive definite, direct rate feedback control can only increase the damping in the system and is always stable.

It is desirable to be able to design the feedback controller to provide specified modal active viscous damping factors, ζ_s^c in mode s, in each of the n_c controlled modes. If ζ_s^c is small (less than roughly 0.3), then one may use the linearized approximation of Aubrun,[14]

$$\sum_i^{n_s} (\phi_{is}^2 d_i) = 2M_s \omega_s \zeta_s^c \quad (\text{for s over } n_c), \tag{26}$$

to relate modal dampings to the feedback constants. For $n_c = n_s$ (number of controlled modes equal to the number of sensor-actuator pairs), Equation 26 can be solved directly for the required d_i (i over n_c). However, this approach can (and usually does) produce negative values for some of the d_i. This result must be avoided, since any $d_i < 0$ will assuredly produce instability in some residual modes.

To avoid negative feedback damping constants, a linear programming approach was developed, with a relaxed requirement on the active damping factors. This approach seeks d_i (i over n_s) such that their sum is minimized, subject to the constraints that all d_i be non-negative and that the resultant dampings be greater than or equal to the specified modal

damping factors. This can be cast into the form of the standard optimization problem as

$$\text{minimize} \quad \sum_{i}^{n_s} d_i$$

$$\text{subject to} \quad \sum_{i}^{n_s} (\phi_{is}^2 \, d_i) \geq 2M_s \omega_s \zeta_s^c, \quad s \text{ over } n_c$$

$$\text{and} \quad d_i \geq 0, \quad i \text{ over } n_s.$$

It may be necessary in some cases to also place an upper bound on $\Sigma(\phi_{is}^2 d_i)$ in order to keep the resultant modal dampings within the linear range of Equation 26, but this was not found to be the case for the application considered in this research.

Using the same transformation as before,

$$\{\dot{q}^s\} = [\Phi^s]\{\dot{\xi}^n\} = [\Phi^a]\{\dot{\xi}^n\},$$

the optimized rate feedback case can be expressed in modal-space equations of motion as

$$[M]\{\ddot{\xi}^n\} + ([D]+[\Phi^a]^T[DF][\Phi^a])\{\dot{\xi}^n\} + [K]\{\xi^n\} = [\Phi]^T\{f^e\}. \qquad (27)$$

The augmented damping matrix becomes

$$[AD] = ([D] + [\Phi^a]^T[DF][\Phi^a]). \qquad (28)$$

It should be noted that this linearized optimization approach is not restricted to $n_c = n_s$, so a direct rate feedback controller could be designed to provide specified minimum dampings in a greater number of controlled modes than the number of sensor-actuator pairs ($n_c \geq n_s$).

Preston and Lin[15] have performed a similar optimization of rate feedback, but with a full matrix containing coupling terms. Their work resulted in a form of modal-space active damping, and they also concluded that colocation was essential to stability.

2.5 CONTROL OF MORE MODES THAN ACTUATORS

A highly desired characteristic of active control of space structures is control of a greater number of modes than the number of actuators used. One approach is to attempt to apply modal-space control to more modes than there are actuators. The requirement that $n_a = n_c$ was brought on by the necessity of a matrix inversion. This requirement can be relaxed if underdetermined or overdetermined systems of linear algebraic equations can be solved by matrix pseudo-inverses.

The first matrix in question here is the $[\Phi^{ac}]^T$ matrix, first appearing in Equation 5. The $[\Phi^{ac}]$ matrix contains the n_a rows of $[\Phi]$ corresponding to actuator locations and the n_c columns corresponding to the controlled modes, and $[\Phi^{ac}]^T$ must be inverted in order to solve for the control matrix which would (ideally) decouple the designated controlled modes. With n_c greater than n_a, $[\Phi^{ac}]^T$ has more rows than columns, and thus describes an over-determined system (more equations than unknowns).

The pseudo-inverse for a non-square matrix [A] in an over-determined system can be obtained through a least-squares solution (as in Brogan[16]) as

$$[A]^{\dagger} = ([A]^{T}[A])^{-1}[A]^{T}, \tag{29}$$

where [A] is m by n and $[A]^{\dagger}$ is n by m with m > n. The matrix pseudo-inverse of $[\Phi^{ac}]^{T}$ is thus given by substitution into Equation 29:

$$([\Phi^{ac}]^{T})^{\dagger} = ([\Phi^{ac}][\Phi^{ac}]^{T})^{-1}[\Phi^{ac}].$$

Because this method is a least-squares solution, using the pseudo-inverse of $[\Phi^{ac}]^{T}$ in the calculation of $[C^{ac}]$ should minimize coupling between controlled modes, at least for any particular set of actuator locations and controlled modes.

To obtain actuator-sensor duality, a greater number of modes than sensors must be sensed. The matrix $[\Phi^{ac}] = [\Phi^{rs}]$ involved in modal estimation by spatial filtering contains more columns than rows for this case, describing an underdetermined system. The pseudo-inverse for this matrix can be defined as

$$[\Phi^{ac}]^{\dagger} = [\Phi^{ac}]^{T}([\Phi^{ac}][\Phi^{ac}]^{T})^{-1}.$$

This definition of a matrix pseudo-inverse can be shown to arise from a minimum norm solution, which is not very meaningful physically in this

estimation and control application. However, this choice creates a symmetric form for the control matrix,

$$[C^{ac}] = -([\Phi^{ac}][\Phi^{ac}]^T)^{-1} [\Phi^{ac}][D^A][\Phi^{ac}]^T([\Phi^{ac}][\Phi^{ac}]^T)^{-1}, \quad (30)$$

which will be negative definite. Elliott et al[10] and Nayak[17] each suggest control and sensing of a greater number of modes than actuators in similar fashion. The total (augmented) system damping matrix is then given by Equation 24 where $[C^{ac}]$ now takes on the form given above in Equation 30 and is still positive definite for a dual control configuration.

2.6 HYBRID CONTROL

It may be desirable in some instances to combine modal space active damping (with spatial filtering) and direct rate feedback control. Since both methods are linear, a combination, or hybrid, control can be developed from superposition of the two separate methods.

2.7 THEORETICAL EIGENSOLUTION AND FREQUENCY RESPONSE CALCULATIONS

Theoretical frequency response calculations and eigenanalysis were performed for the open-loop and closed-loop systems using methods which were naturally quite similar to those used in References 7 and 8, although the formulation here is simpler, owing to the lack of additional dynamic elements (the spectral filters). For the solution of the closed-loop eigenvalues, a general homogeneous equation can be written,

$$[M]\{\ddot{\xi}^n\} + [AD]\{\dot{\xi}^n\} + [K]\{\xi^n\} = \{0\}, \tag{31}$$

where [AD] represents a total damping matrix (in the modal-space), including both inherent and active damping. This matrix can take on any of the forms presented in this chapter (with the exception of the spectral filtering approach). Alternatively, [AD] can be set equal to just the inherent damping matrix in order to model the open-loop system. A 2n by 1 state vector, {x}, is formed from the modal states as

$$\{x\} = \begin{Bmatrix} \{\dot{\xi}^n\} \\ \{\xi^n\} \end{Bmatrix}.$$

Further, an auxiliary equation of the form

$$[M]\{\dot{\xi}^n\} - [M]\{\dot{\xi}^n\} = \{0\}$$

allows the formulation of a state-space system of order 2n, as

$$[B]\{\dot{x}\} - [A]\{x\} = \{0\} \tag{32}$$

where

$$[B] = \begin{bmatrix} [0] & [M] \\ [M] & [AD] \end{bmatrix}$$

and

$$[A] = \begin{bmatrix} [M] & [0] \\ [0] & -[K] \end{bmatrix}.$$

The system roots are then the complex eigenvalues, p, of

$$p[B]\{x\} = [A]\{x\}.$$

For each complex conjugate pair, $p = \sigma \pm i\omega$, one can define a damping factor,

$$\zeta = \frac{-\sigma}{\sqrt{\sigma^2 + \omega^2}},$$

and a frequency,

$$f = \frac{\sqrt{\sigma^2 + \omega^2}}{2\pi}.$$

The frequency response analysis was accomplished by allowing for the nonhomogeneous form of Equation 31,

$$[M]\{\ddot{\xi}^n\} + [AD]\{\dot{\xi}^n\} + [K]\{\xi^n\} = [\Phi]^T\{f^e\}, \tag{33}$$

where $\{f^e\}$ is an excitation vector, with only one nonzero term. For harmonic excitation at frequency ω, in DOF k, Equation 33 reduces to

$$(-\omega^2[M] + i\omega[AD] + [K])\{\Xi^n\} = \{F_k^e\}, \tag{34}$$

where $\{F_k^e\}$ is the k^{th} column of $[\Phi^a]^T$, and $\{\Xi^n\}$ represents the vector of frequency response in modal coordinates. The vector $\{\Xi^n(\omega)\}$ is then obtained by direct solution of Equation 34 at various values of ω. The

complex displacement FRF for response in DOF j due to excitation at DOF k can then be obtained using the modal expansion equation (Equation 4) as

$$DFRF_{j,k}(\omega) = [\Phi_j]\{\Xi^n\} \tag{35}$$

where $[\Phi_j]$ is the j^{th} row of $[\Phi]$. The velocity FRF can then be obtained by

$$VFRF_{j,k}(\omega) = i\omega(DFRF_{j,k}(\omega)).$$

2.8 COMPUTER CODES

Fortran computer codes were developed by the author, for the IBM 370 system at VPI&SU which perform all of the theoretical calculations described in this chapter. One set of programs calculates the control matrix, $[C^{ac}]$, based upon spectral or spatial filtering. Another program solves the linear programming problem for the optimized rate feedback gains and creates a control matrix analogous to $[C^{ac}]$. Another set of programs can be used to calculate the closed-loop system complex roots, or the closed-loop frequency response for any structural DOF. The common input to all of the programs is the structural dynamic data, consisting of generalized mass, damping, and stiffness parameters and the modal matrix, which were developed with finite element techniques of previously existing software and correlated with open-loop experiments. The programs which calclulate the control matrix generate a data set which

includes all control parameters, including the actuator and sensor locations and target modes, as well as the newly calculated feedback gains. This data set can then be used as input to the roots and FRF programs.

Theoretical results which will be shown in later chapters were developed with this software.

3.0 LABORATORY MODELS

In order to evaluate various active vibration control theories and techniques, laboratory models are required which possess some of the structural dynamic characteristics of large flexible space structures. An ideal model would exhibit low frequency modes and a high modal density, with perhaps a pair or pairs of very close modes. A space structure will naturally have several rigid body modes, but it is extremely difficult to produce such rigid body modes within the earth's gravitational field. Also, it is difficult to reproduce the vacuum of space in a small earth-based laboratory. Such exotic conditions would be more properly addressed by on-orbit experiments. Ground-based laboratory studies are better suited to control of low-amplitude vibrations of non-zero frequency, with an emphasis placed on gaining a practical understanding of the interaction of active vibration control strategies and a well-modeled, well-behaved structure.

With these goals in mind, the present study involved three relatively simple laboratory models. The first consisted of a flexible steel beam suspended vertically by taut cables; this will be referred to as the beam-cable structure. Another model resulted from a modification to the first structure with a horizontal aluminum beam attached to the vertical steel beam to form the cruciform beam structure. An entirely different model, which will be referred to as the hanging grid structure, was comprised of a flexible aluminum plane grid structure suspended from a steel top beam in rotational bearings. Each structure had several

interesting characteristics of its own, which will be discussed in the following sections.

3.1 BEAM-CABLE STRUCTURE

The beam-cable structure, which has been the subject of a previous Master's thesis[6] and several other papers,[7,19,20] was fashioned from an 80-inch long steel beam suspended vertically by four steel cables in tension, as shown in Figures 1 and 2. The beam had a uniform rectangular cross section, 2 inches wide and 1/8 inch thick, with the 2-inch dimension in the plane formed by the 0.09-inch diameter suspension cables. The line drawing of Figure 2 gives the overall dimensions of the structure. The sectional bending modulus (EI) was experimentally determined[18] to be 9060 lb-in^2. For all intents and purposes, all structure-borne hardware, such as cable clamps and actuator/sensor coil assemblies were considered as part of the structure.

This structure was intended to be a relatively mild test of active control systems and was therefore designed to have several low frequency modes, but no true rigid body modes or closely spaced modes. The structure was represented accurately by an 18-dof finite element model, including consistent mass and stiffness matrices and a geometric stiffness matrix accounting for the effects of tension in the beam. Greater detail on the structure and the math model can be found in Skidmore[6].

Experimentally measured and theoretically predicted natural frequencies were well within five percent agreement for the first five modes, as shown in Figure 3. Satisfaction of the design goal was achieved

with five interesting modes below 30 Hz. As the mode shapes in Figure 3 indicate, the beam participated as a quasi-rigid body in the first two modes, with the cables undergoing the majority of the deformation. All higher modes demonstrated much greater beam flexure.

3.2 CRUCIFORM BEAM STRUCTURE

The structure described in the preceding section was modified in an attempt to increase the dynamic complexity of the model. The change consisted of adding a 32-inch long aluminum crossbeam with tip masses, clamped perpendicular to the existing structure, as depicted in Figure 4. This additional beam was also 2 inches wide by 1/8 inch thick and possessed a sectional modulus (EI) of 2680 lb-in^2.[18]

The modification had the effect of adding a new mode, within 1 Hz of the original third mode, while the remaining low frequency modes had the expected decrease in frequency due to the increased mass. The natural modes, calculated in a similar fashion to the previous model, are shown in Figure 5. Much greater detail regarding the structure, math model, and modes can be found in Schamel[18].

3.3 HANGING GRID STRUCTURE

The primary test structure for this study was the hanging grid structure, originally designed by Masse[21] and later modified and analyzed by Gehling[22]. The grid shown in Figures 6 and 7 was the most challenging and most interesting of the models discussed here. This structure was also the subject of Reference 8.

As depicted in Figure 7, a compound beam made of steel was mounted horizontally in two pillow-block bearing supports, to allow frictionless rotation. A plane grillage, made up of flexible aluminum bars, was suspended from this top beam in the shape of a parallelogram with variable skew angle with respect to the vertical. In addition, two large eccentric masses were positioned at the ends of the top beam. The rotational bearing support, together with the adjustable-offset of the eccentric masses, allowed a variable, low frequency pendulum mode of the structure, which was similar in nature to a rigid body mode, although of non-zero frequency. Moreover, the flexibility of the aluminum grillage provided for many low frequency modes and a high modal density. A grillage skew angle of 46 degrees was chosen for this study, for consistency with the data obtained by Gehling[22].

Gehling[22] used a 58-DOF finite element model with frame elements for the grillage. Excellent agreement between theory and experiment for both frequencies and mode shapes was obtained once a geometric stiffness matrix was included, accounting for tension, shear and bending moment in each element.[23] Theoretical and experimental natural frequencies are listed in Table 1.

Table 1. Natural frequencies of hanging grid structure

Mode r	Theoretical f_r(Hz)	Experimental f_r(Hz)
1	0.581	0.596
2	0.870	0.886
3	1.349	1.37
4	3.190	3.18
5	3.488	3.46
6	4.850	4.92
7	5.483	5.45
8	5.645	5.57
9	5.952	6.11
10	7.898	7.83
11	8.182	8.13
12	9.006	8.99
13	9.457	9.43
14	11.20	11.2
15	12.87	13.2
16	20.56	----
17	24.09	24.4
18	26.37	25.3
19	28.23	27.1
20	29.81	27.6
21	-----	28.6
22	-----	30.1

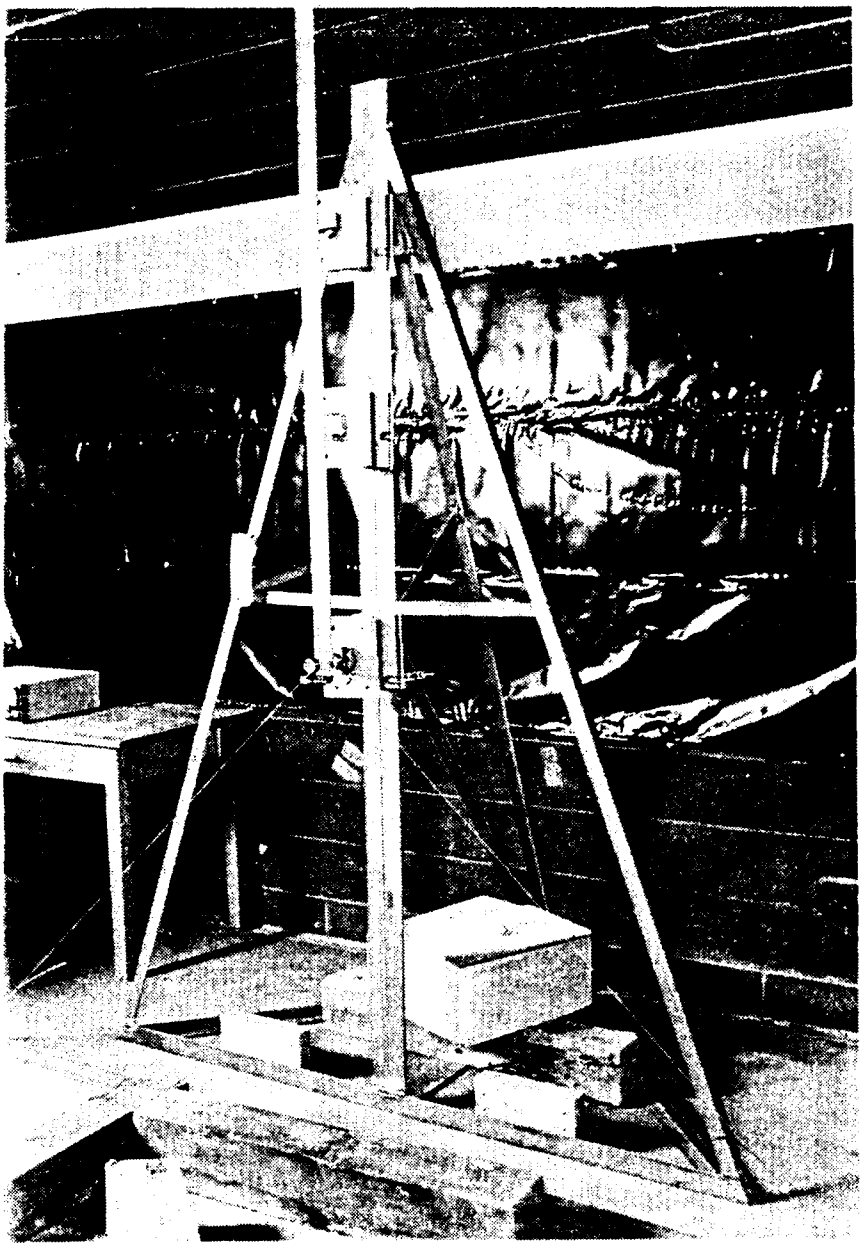

Figure 1. Photograph of beam-cable structure

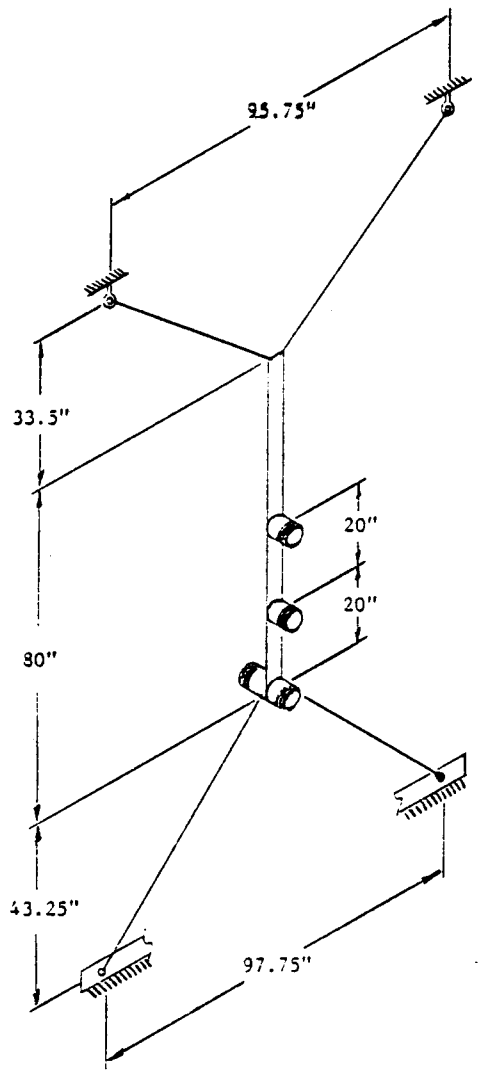

Figure 2. Drawing of beam-cable structure

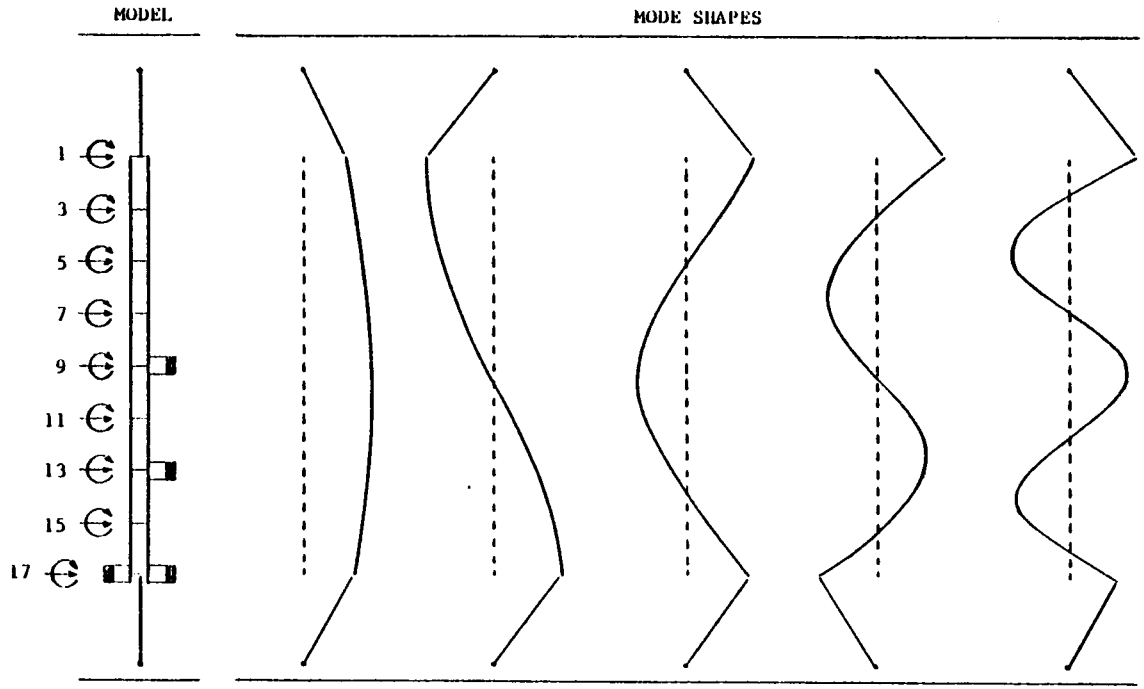

	Mode	1	2	3	4	5
Freq. (Hz)	Theory	2.24	5.27	9.34	15.5	24.6
	Exper.	2.24	5.25	9.30	15.3	23.8

Figure 3. Modes of beam-cable structure: Experimental frequencies and theoretical frequencies and mode shapes.

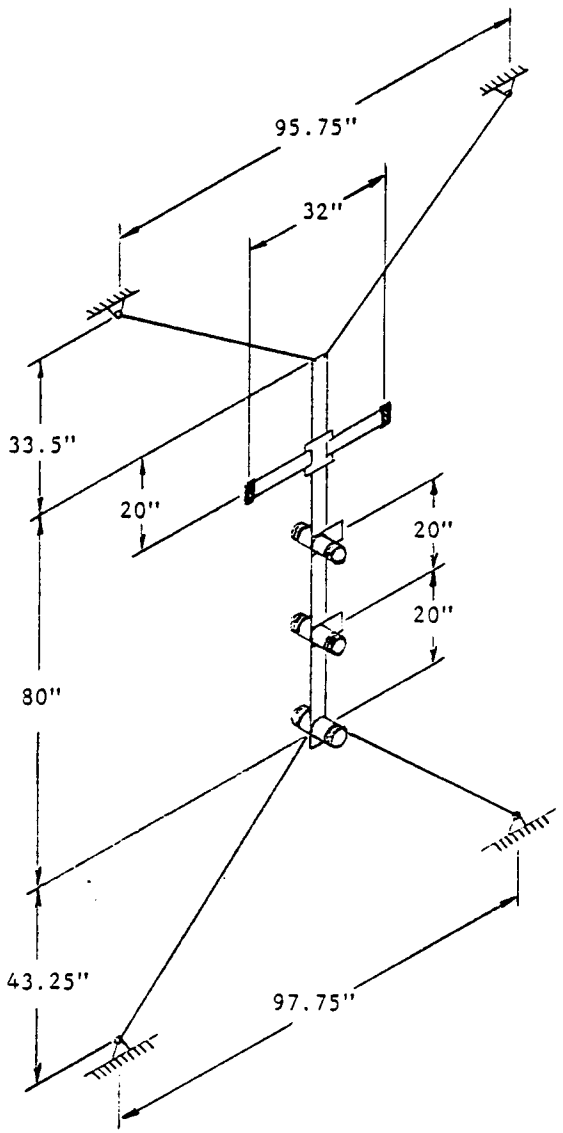

Figure 4. Drawing of cruciform beam structure

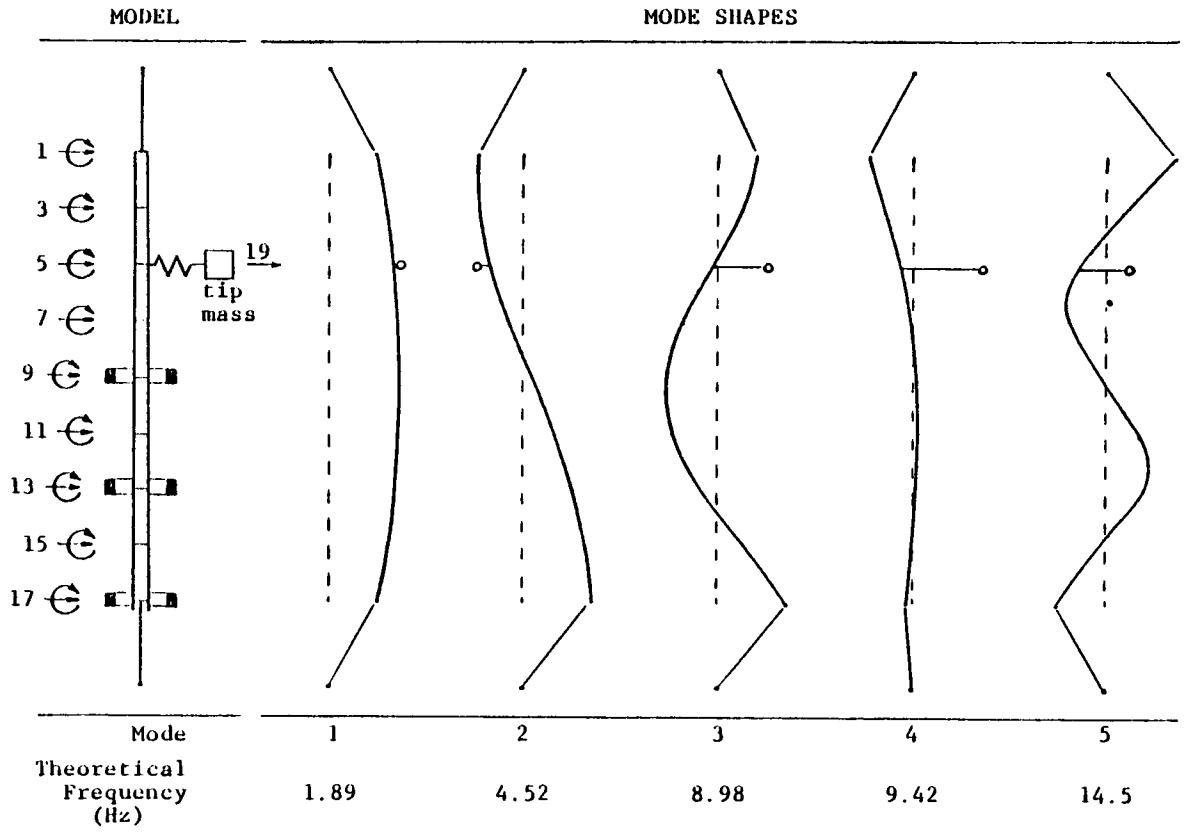

Figure 5. Modes of cruciform beam structure: Experimental frequencies and theoretical frequencies and mode shapes.

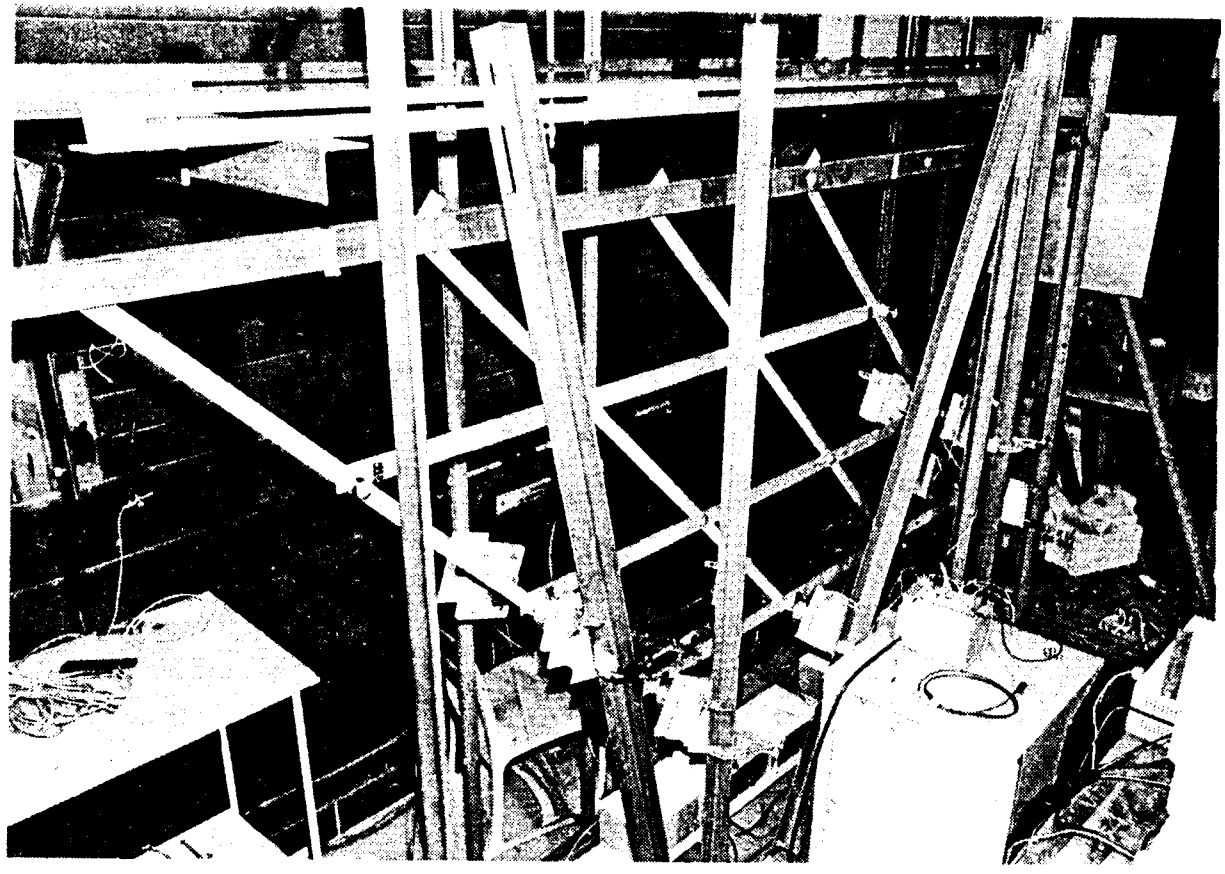

Figure 6. Photograph of hanging grid structure: photograph by Mark Hill, courtesy of ENGINEER'S FORUM Magazine of VPI&SU.

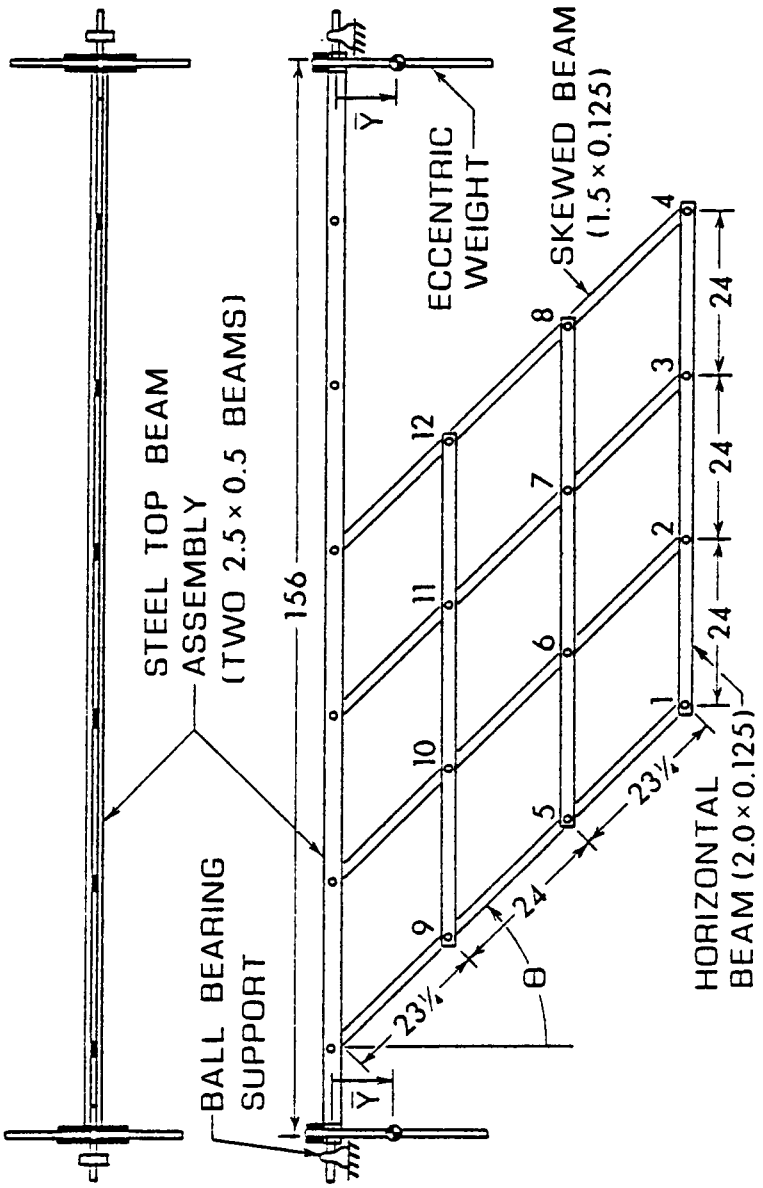

Figure 7. Drawing of hanging grid structure

4.0 EXPERIMENTAL IMPLEMENTATION

The design, analysis, operation, and performance of active control is critically dependent on the hardware available to create the architecture of the control system. This hardware typically consists of sensors and actuators, and the controller which links them. For actual space structures, sensors will be of two varieties, either structure-borne (such as accelerometers) or remote (optical sensors). Also, the actuators are likely to be structure-borne (reaction control thrusters, proof-mass actuators, or control moment gyroscopes), since there is no fixed support to push against in space. However, these systems involve many complicating factors, such as complex actuator dynamics or the need to integrate an acceleration signal, which could tend to obscure the analysis and results of a preliminary validation of a promising control concept.

4.1 SENSOR-ACTUATOR DESIGN

To avoid the complications of structure-borne sensors and actuators, this study employed simple, mechanically grounded, non-contacting velocity sensors and control force actuators, which have been used extensively in previous studies.[6-8,18-22] The sensors and actuators are of similar electro-magnetic design and are pictured in Figure 8. Each unit consisted of a structure-borne conducting coil interacting with a stationary magnetic field structure, which was attached to an external support framework. All field structures were mounted on adjustable bases

to aid in the positioning process during system set-up. The velocity sensors provided relatively strong signals that were linear (over a small range) and had no DC offset. The force actuators, driven by specially designed, controlled-current power amplifiers, provided forces which were directly proportional to the control input voltages.

More detail regarding design and performance of the sensors, actuators, and power amplifiers is available in References 6 and 20.

4.2 CONTROLLERS

4.2.1 ANALOG CIRCUITRY

Analog circuits were used in the first attempts at modal-space control, primarily for such functions as spectral filtering and application of control gains. For the spectral filtering case, the band-pass filter design of Forward[11] was implemented with analog circuits, as detailed in Reference 6. and described in Chapter 2. Each element of the control matrix $[C^{ac}]$ was represented by a separate gain circuit, and appropriate signals were added with summation circuits before being sent on to the force actuators' power amps. In addition, each velocity sensor required a high input impedance buffer amplifier to prevent current leakage through the coil. This was accomplished with voltage follower circuits using high impedance LF353 Bi-FET operational amplifiers.

4.2.2 DIGITAL CONTROLLER

The acquisition of a PC-1000 programmable digital control computer (from Systolic Systems, Inc. of San Jose, California) permitted

replacement of most of the analog circuitry involved in previous research - at a great saving of time involved in wiring the circuits. However, the velocity sensors still required a high-input impedance voltage follower, which had to be analog and external to the control computer. The PC-1000 system, which operates through an IBM personal computer, consists of a 16-channel data acquisition system (with 2000 Hz sampling rate capability), a high-speed array processor, and 16 output channels for control or data signals. The PC-1000 and its host IBM-PC are shown in the foreground of Figure 9. The array processor performs the multiplication of a fully programmable system matrix times a vector made up of the input signals and internal state variables. The result of this multiplication consists of the updated state variables and the output signals.

It was assumed that with a high sampling rate (2000 Hz) and a high throughput rate (array processor operation time), the digital controller could satisfactorily approximate a continuous time system. Therefore, the PC-1000 was used to implement the control gains calculated for a continuous time controller. The programmability of the unit greatly facilitated the implementation of the various forms of control and permitted easy changes between control methods. It also provided a simple but effective means of activating a control method with its run/halt switch.

4.3 DATA ACQUISITION

Experimental data was acquired using an STI-11/23 data acquisition-analysis system developed by Synergistic Technology

Incorporated of Cupertino, California. This system generated excitation signals for frequency response measurements and acquired and processed the data signals.

Frequency responses, which form the bulk of the experimental results in this study, could be measured in three different ways: slow, incremental sine sweeps; fast chirp sine sweeps; or random-phased spectrum tests. Random-phased spectrum excitation is developed from a constant magnitude spectrum with random phase angle which is transformed into a temporal excitation signal that has the characteristics of white noise and should excite all structural frequencies. Excitation signals could be input to the structure using any one of the control force actuators, taking advantage of the linearity of the actuator system to use it simultaneously as a vibration exciter and an active controller. Experimental data was processed in the form of frequency response functions generated by the STI-11/23.

The STI-11/23 also has the capability of performing a curve-fit procedure, using displacement frequency response functions. This displacement data could be either measured directly or obtained by a frequency-domain integration of velocity frequency response functions. The procedure assumes non-coupling modal viscous damping, and allows for inclusion of residuals to permit multi-mode curve-fits. Data could be obtained from several sensor locations and processed to arrive at globally averaged curve-fit parameters. The results of this analysis were experimental values for frequency and damping ratio.

A block diagram of a typical experimental configuration is given in Figure 10.

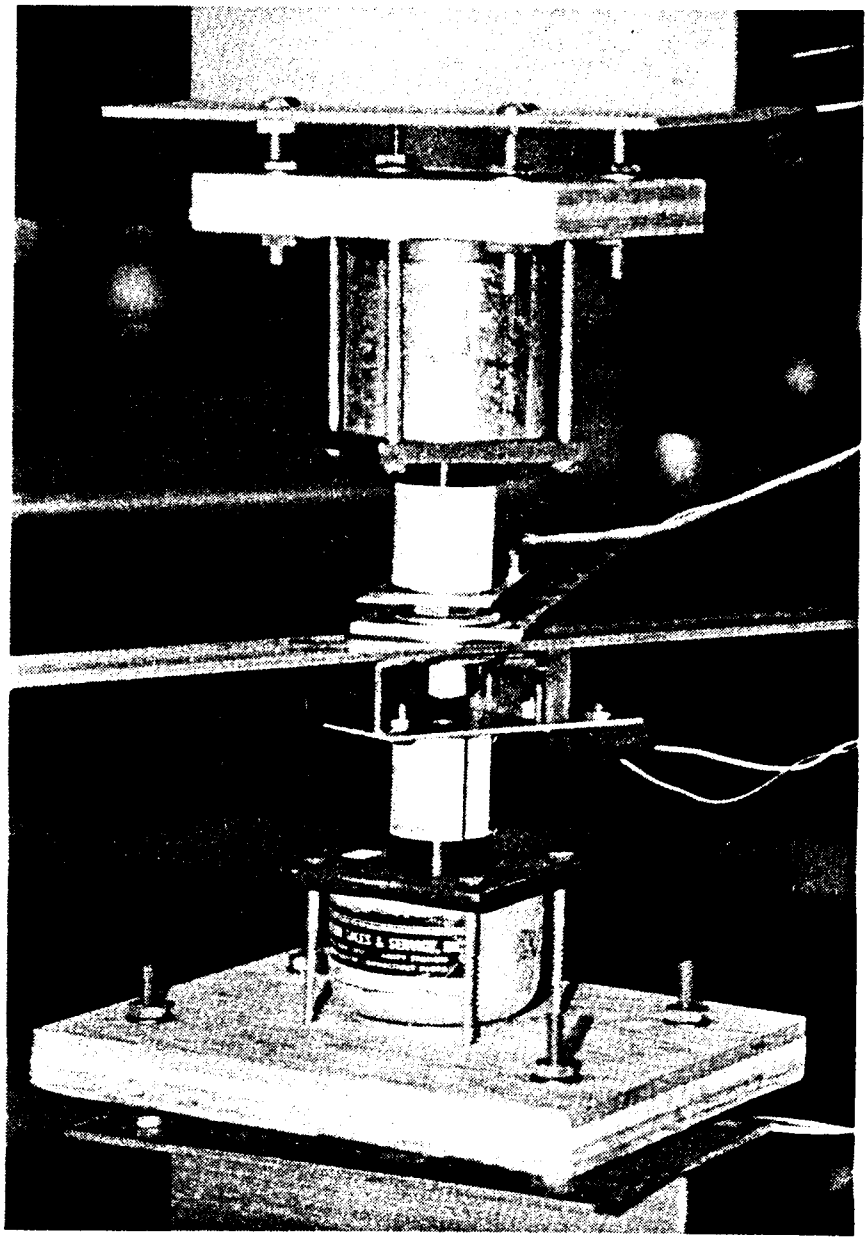

Figure 8. Photograph of sensor-actuator pair: Photo is of joint 5 of hanging grid structure.

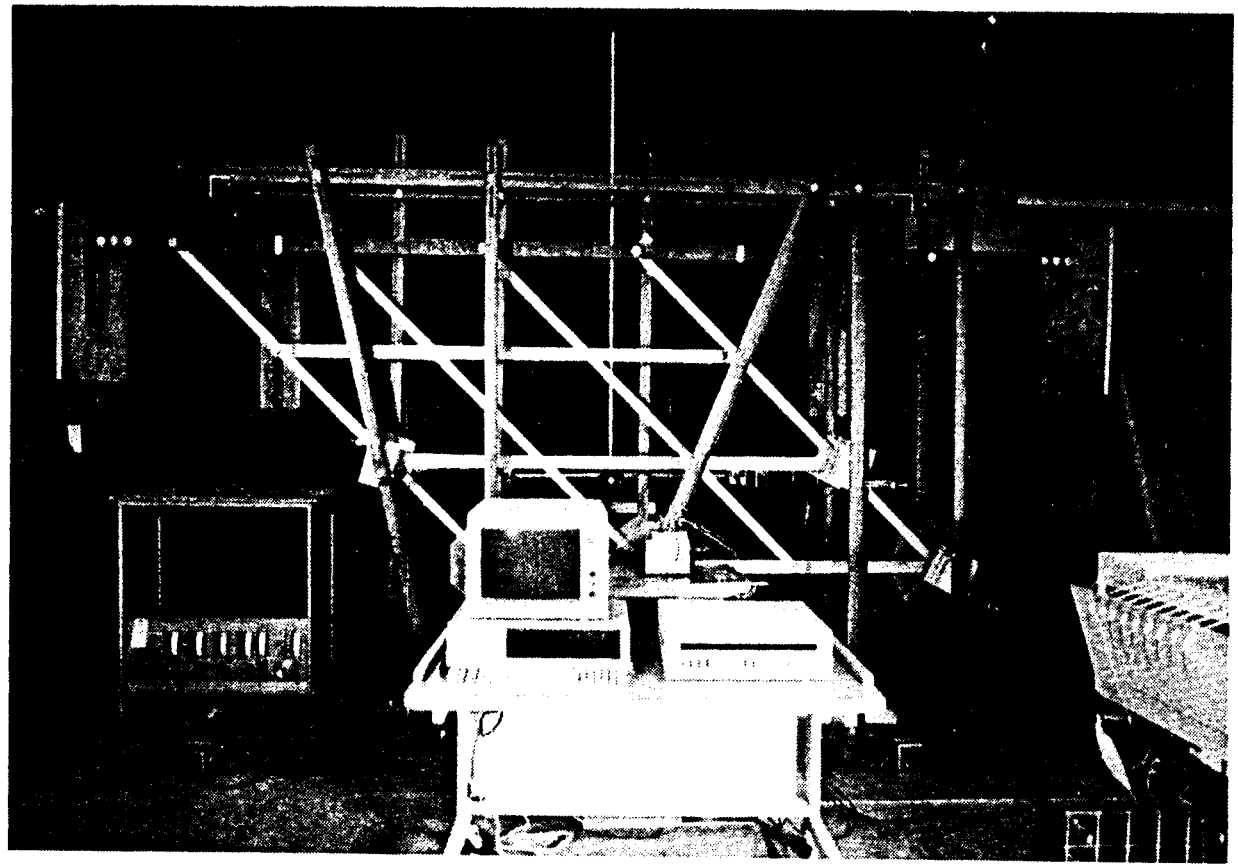

Figure 9. Photograph of PC-1000 and IBM-PC: Hanging grid structure is shown in background.

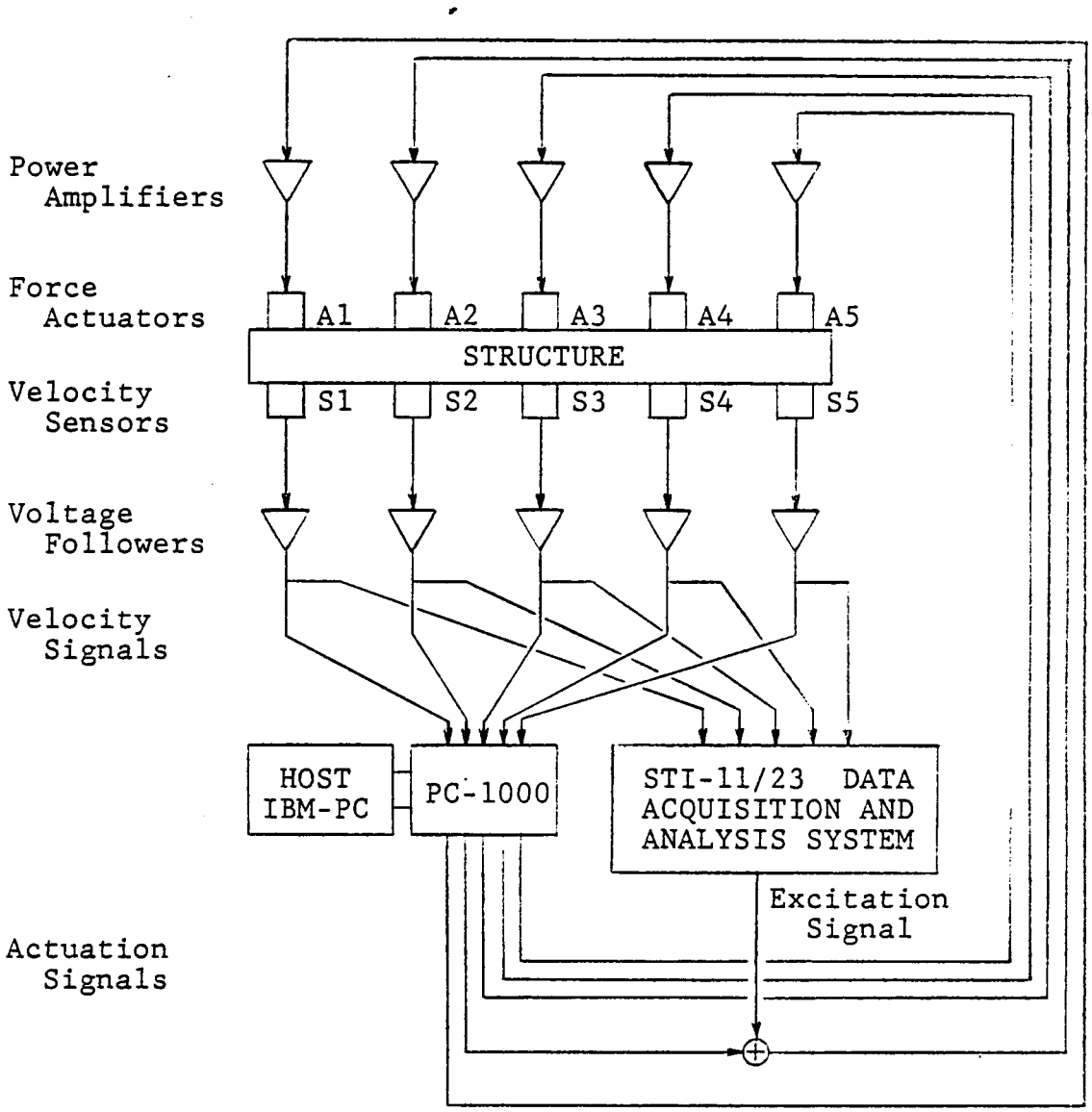

Figure 10. Block diagram of control/data acquisition systems

5.0 RESULTS OF SPECTRAL FILTERING EXPERIMENTS

Modal-space active damping with spectral filtering for modal identification (see Section 2.2) was implemented on both the beam-cable structure and the hanging grid structure with somewhat limited success. Damping was enhanced by the control, but not to the degree originally expected, nor in the manner expected. The results of these tests were first published in References 6, 7, and 8. The relevant findings are summarized here, and the different reports are related and compared for the first time.

The author's first implementation of modal-space active damping with spectral filtering involved the beam-cable structure. The first three modes of the structure were selected for the controlled modes, with target active viscous damping factors of 0.1 (10% damping) in each mode. Hardware availablity at the time (early 1983) dictated that only three modes could be actively controlled. The filters were designed for bandwidths of 1.0 Hz, while the minimum modal separation was approximately 3.0 Hz. The experimental results, along with a rough attempt at the corresponding theoretical analysis, formed the basis for the author's Master's thesis.[6] In the initial study, data consisted of transient responses to several sets of displacement initial conditions.

As reproduced from Reference 6, Figure 11 shows the Fast Fourier Transforms (FFTs) of open-loop and closed-loop experimental transient response at the lower end of the beam (in terms of velocity), and also the theoretically predicted closed-loop response (solid curve). The initial condition which produced this response was a displacement state

that roughly approximated the third mode. When released from this state, the structure exhibited significant response in all of the low modes. The plot covers the frequency range from 0 to 10 Hz, which shows only the first three modes. The dominant characteristic of the experimental response in the frequency domain was the pair of peaks in the closed-loop data which bracketed the original structural resonance of each controlled mode. The over-simplified theoretical model in use at the time could not predict this unusual behavior, as can be seen in Figure 11. However, it was obvious from the decreased amplitude of motion at resonance (in the experimental data) that damping was increased, although the target damping level of 0.1 could not be verified. It should also be noted that all residual modes (although not shown in this figure) were observed to be damped slightly by the application of control, or at worst, were left unaffected.

The extreme mismatch between experiment and theory in the closed-loop data indicated a need for refinements in the modeling process. The experimental data suggested that each original structural root (eigenvalue) corresponding to a controlled mode had been split into two new closed-loop system roots. This occurrence had not been anticipated, and the mechanism of this behavior was unclear.

Further experimental work which dealt with frequency response behavior of the beam-cable structure, using the same control system, showed closed-loop behavior similar to that in the transient response case; two closed-loop peaks bracketed each controlled mode's original open-loop resonance. It was suspected that the dynamic behavior of the spectral filters were contributing to this occurrence, and subsequent analysis

revealed the coupling between the filters and the structure, as described mathematically in Section 2.2. The corrected theory led to theoretical frequency response functions (FRFs) which were better correlated with experimental FRFs. This data, and the corresponding analysis, formed the basis for Reference 7. Figure 12, as reproduced from that paper, shows the measured velocity FRF (VFRF) of the beam-cable structure for both open- and closed-loop systems, which relates velocity at the bottom of the beam (DOF 17) in response to excitation 10 inches above the bottom (DOF 15, refer to Figure 3 for DOF numbering) for the frequency range 0 to 10 Hz. In the figure, solid lines denote closed-loop response, and broken lines denote open-loop response. Comparison with Figure 13 (also from Reference 7), which gives the corresponding theoretical VFRFs, shows the good agreement obtained between theory and experiment. Table 2 lists the open- and closed-loop system roots (eigenvalues) in terms of frequency and damping ratio. The open-loop damping ratios were determined approximately from a process of matching theoretical and experimental open-loop frequency responses. This involved an iterative procedure, comparing the peak magnitudes in calculated and measured frequency responses and adjusting the damping ratio until reasonably close agreement was achieved. The closed-loop damping ratios resulted from an eigenanalysis which included these approximated open-loop damping values. This data reveals that each of the two closed-loop frequency response peaks bracketing the original open-loop resonance corresponded to a new system root - one for the structural mode and one for the spectral filter corresponding to that mode. The frequencies at which the closed-loop

peaks occurred match the closed-loop roots' frequencies as listed in Table 2.

Modal-space active damping with spectral filtering was later applied to the hanging grid structure. This experiment and corresponding theoretical analysis were first reported in Reference 8. Using five control force actuators, five modes were targeted to receive 0.1 damping. The set of controlled modes consisted of modes 2, 3, 4, 5, and 6, which represented a consecutive sequence of low frequency modes excluding the first, pendulum, mode. This set included the first pair of closely-spaced modes (4 and 5), at 3.4 and 3.7 Hz. The solitary control sensor, which measured out-of-plane velocity, was positioned at joint 1 (see Figure 7 for joint numbering). The five actuator locations, at joints 1, 2, 4, 5, and 8, were chosen after using the theoretical model to evaluate several possible sets of actuator locations for grid points 1 through 8. A formal optimization procedure was not deemed necessary.

The bandpass filter for each controlled mode was centered on the mode's experimentally measured natural frequency. The filters for modes 2, 3, and 6 were given bandwidths of 1.0 Hz, while those for modes 4 and 5 were narrowed to 0.33 Hz. These two filters were made more narrow because modes 4 and 5 were the closely-spaced pair of modes, with a frequency separation of only 0.3 Hz.

When this controller was first activated, the structure-control system exhibited a mild dynamic instability at roughly 3.5 Hz, in the neighborhood of the two closely-spaced modes (as well as the two closely-spaced filters). A trial-and-error process of disabling the control for individual modes produced a stable system when the control

for mode 5 was deactivated. In this case, modes 2, 3, 4, and 6 were actively damped by five actuators and one velocity sensor.

Table 3, as reproduced from Reference 8, lists the resultant open- and closed- loop system roots. Here again, open-loop damping ratios were experimentally determined by matching measured and calculated frequency responses, and closed-loop damping ratios are theoretical values. The two closed-loop structure-control systems refer to the unstable 5-mode controller and the stable 4-mode controller. The negative damping value of system root 7 for the 5-mode controller accurately predicts the 3.5 Hz instability which was observed experimentally.

Experimental frequency responses were measured directly in slow, incremental sine sweeps. Due to the instability in the 5-mode control case, the only closed-loop data is for the 4-mode controller. A noncontacting displacement sensor was located at joint 2, in order to measure the driving point displacement frequency response function, as excitation was introduced to the structure through the force actuator located at this point. The resulting experimental data and the corresponding theoretical analysis are presented in Figure 14 (solid curves are used to indicate closed-loop data). Comparison of the open- and closed- loop experimental data shows the active damping applied to modes 2, 3, 4, and 6 and the relative lack of damping in mode 5. Mode 1 can be seen to have received a large amount of damping due to beneficial control spillover, as predicted by the theoretical frequency response analysis (and also the theoretical roots of Table 3). The theoretical DFRF presented in Figure 14 shows the degree of correlation which was achieved between experiment and theory. It should be noted that the

discrepancy between the two plots in the levels of modes 6, 7, and 8 is due to mode shape errors, which are amplified by the logarithmic scaling. The double resonance behavior which was observed on the beam-cable structure was not readily apparent for the hanging grid structure. This can be explained by the closeness of certain pairs of roots (4-mode controller roots 3 and 4, and 8 and 9, as listed in Table 3) which would cause them to appear as only one root in the plotted frequency responses. Also, system root 5 was so heavily damped that it would not show up in the frequency response.

The structural modes which had been targeted to receive 0.1 damping were not this heavily damped by the controller. Referring again to Table 3, one can see that the largest level of damping in a controlled mode was a level of 0.074 in structural mode 2 (system root 2). All other controlled modes had a damping factor of roughly 0.05. This deficiency was explained in detail in Reference 8 to have resulted from the dominance of the dynamic behavior of the spectral filters. A detailed theoretical analysis in that reference suggested that the closed-loop damping ratio for a controlled mode would be more dependent on the design of the spectral filter than on the damping specified on the basis of ideal modal-space control.

Table 2. System roots of beam-cable structure with spectral filtering

System Mode r	Type*	Open-loop f_r(Hz)	Open-loop ζ_r	Closed-loop f_r(Hz)	Closed-loop ζ_r
1	SM 1	2.24	0.0055	2.01	0.116
2	FM 1	2.24	0.223	2.48	0.110
3	SM 2	5.27	0.0037	4.86	0.046
4	FM 2	5.27	0.0949	5.81	0.053
5	SM 3	9.34	0.0037	8.60	0.031
6	FM 3	9.34	0.0535	9.92	0.024
7	SM 4	15.5	0.0050	15.7	0.0060
8	SM 5	24.6	0.0050	24.6	0.0051
9	SM 6	38.3	0.0051	38.3	0.0051

* SM s - denotes structure mode s
FM s - denotes filter for structure mode s

Table 3. System roots of hanging grid structure with spectral filtering

System Mode r	Type*	Open-loop f_r(Hz)	Open-loop ζ_r	Closed-loop 5-Mode Control f_r(Hz)	Closed-loop 5-Mode Control ζ_r	Closed-loop 4-Mode Control f_r(Hz)	Closed-loop 4-Mode Control ζ_r
1	SM 1	0.597	0.043	0.421	0.153	0.421	0.153
2	SM 2	0.965	0.050	0.913	0.074	0.914	0.074
3	FM 2	0.965	0.518	1.296	0.425	1.294	0.425
4	SM 3	1.432	0.035	1.290	0.046	1.290	0.048
5	FM 3	1.432	0.349	1.809	0.221	1.798	0.219
6	SM 4	3.413	0.010	3.104	0.026	3.156	0.027
7	FM 4	3.413	0.049	3.559	-0.010	3.675	0.029
8	SM 5	3.728	0.009	3.561	0.068	3.728	0.009
9	FM 5	3.728	0.045	3.987	0.022.	3.728	0.045
10	SM 6	5.151	0.013	4.680	0.058	4.654	0.056
11	FM 6	5.151	0.097	5.640	0.041	5.659	0.047
12	SM 7	5.494	0.0035	5.480	0.011	5.478	0.0068
13	SM 8	5.667	0.0030	5.666	0.0044	5.666	0.0041
14	SM 9	6.630	0.0060	6.747	0.0092	6.658	0.0080
15	SM 10	8.618	0.0060	8.642	0.0061	8.615	0.0060

* SM s - denotes structure mode s
FM s - denotes filter for structure mode s

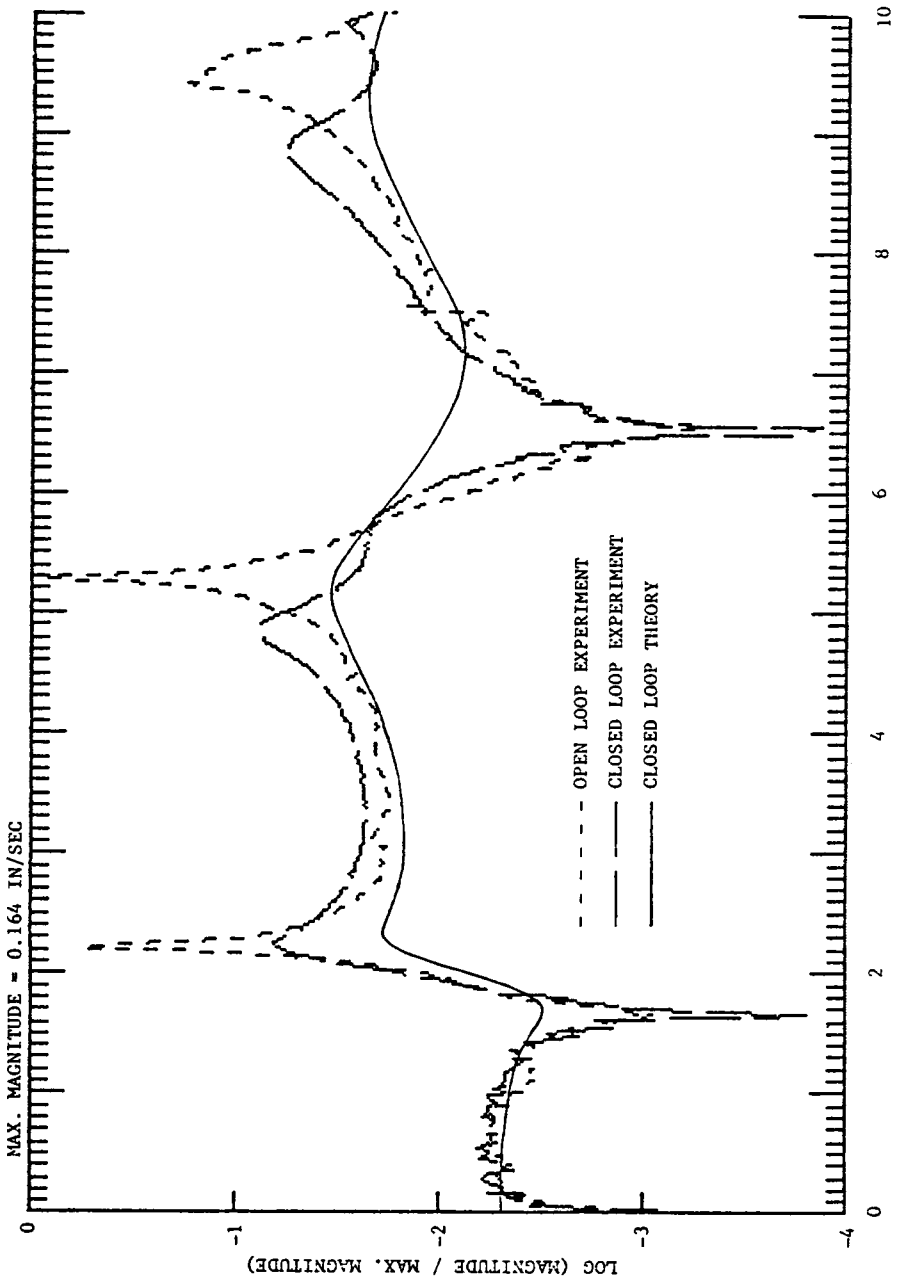

Figure 11. FFT of transient response of beam-cable: Fast Fourier Transforms of velocity response to dispalcement initial conditions; measurement at bottom of beam (0.025 Hz resolution).

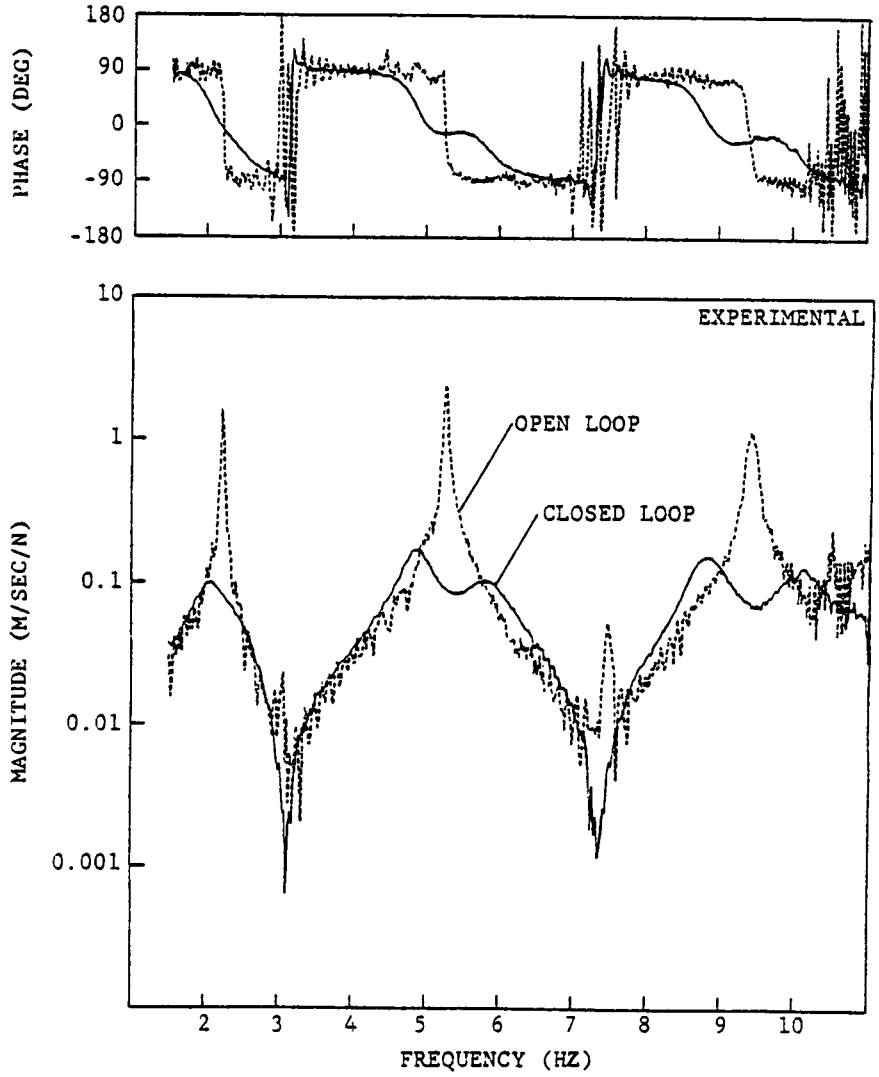

Figure 12. Experimental VFRF of beam-cable with spectral filtering: Solid line gives closed-loop response with modal-space active damping (0.025 Hz resolution).

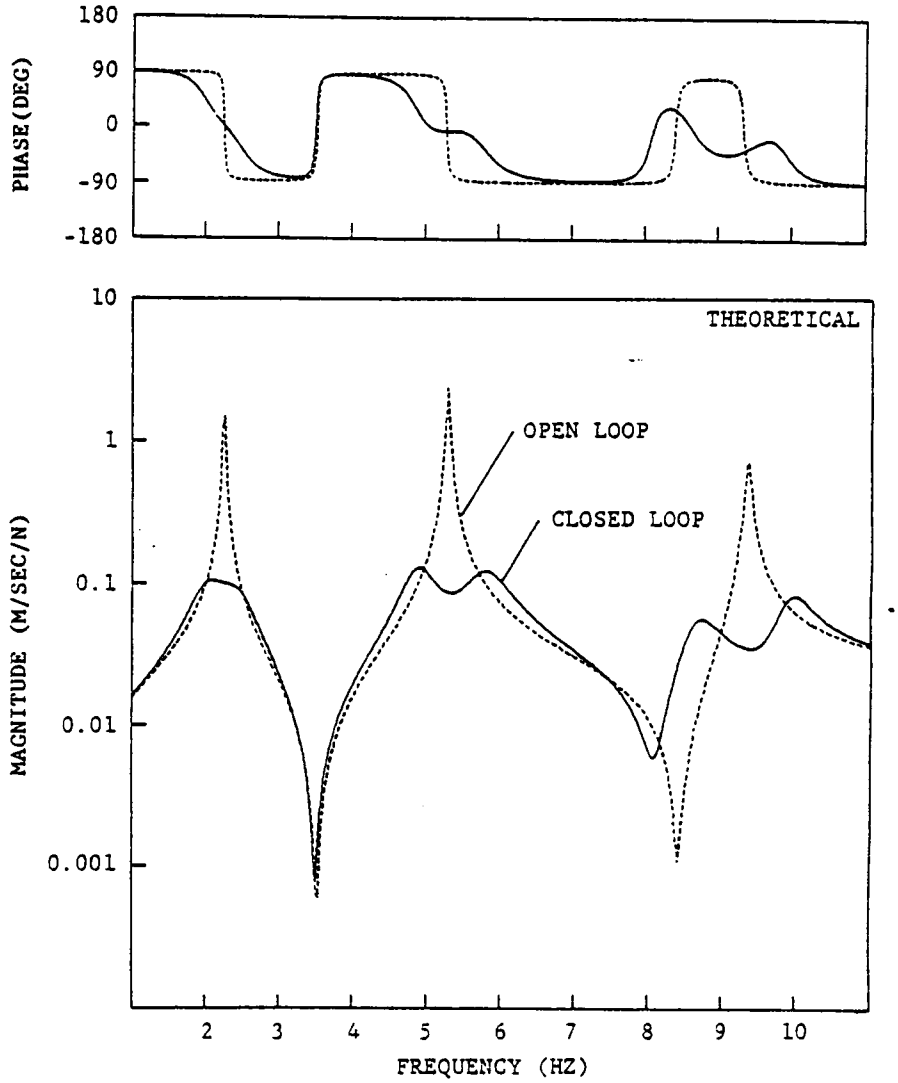

Figure 13. Theoretical VFRF of beam-cable with spectral filtering: Solid line gives closed-loop response with modal-space active damping (0.025 Hz resolution).

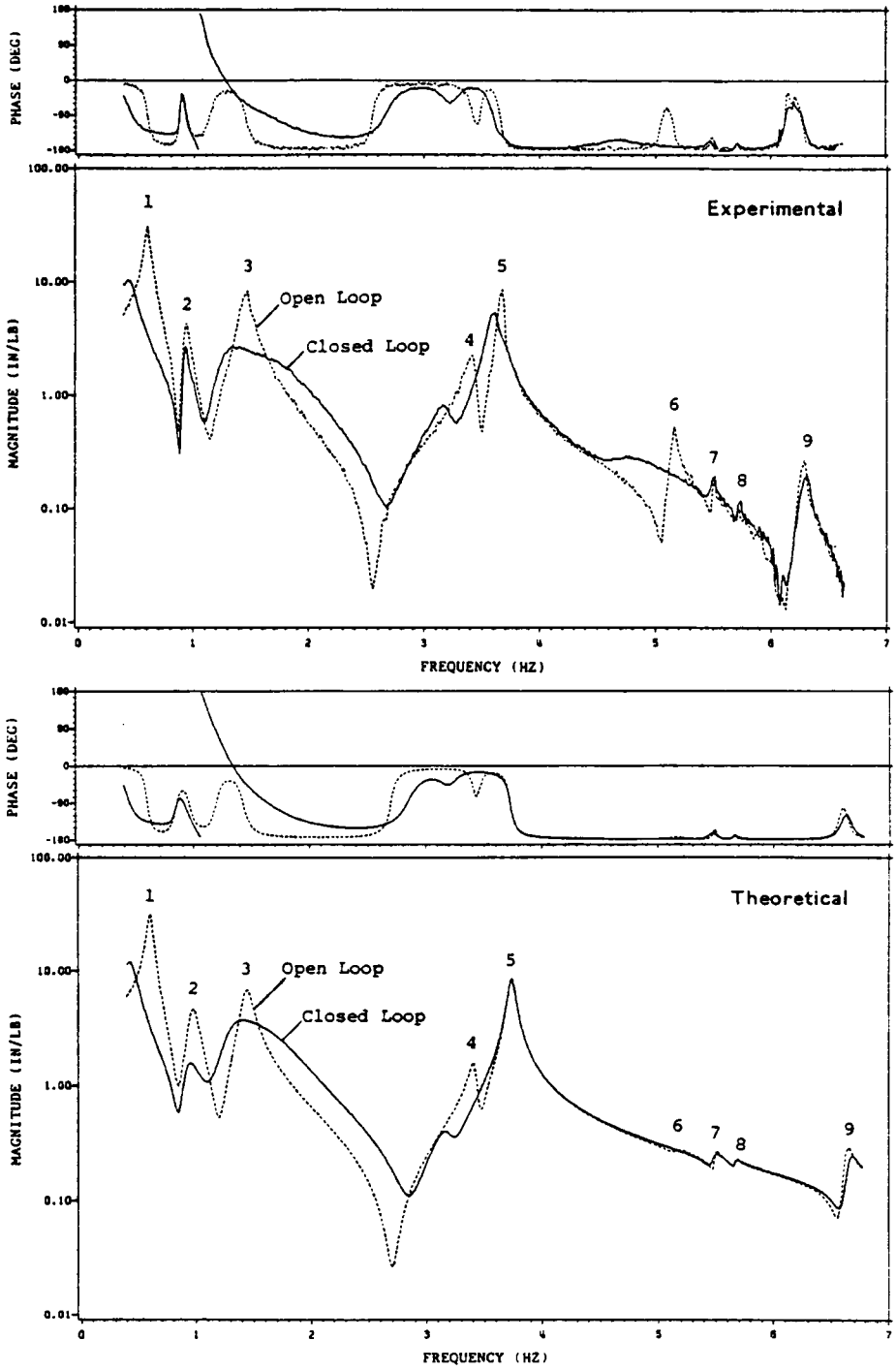

Figure 14. DFRF(2,2) of hanging grid with spectral filtering: Closed-loop data is for stable 4-mode modal-space control (0.025 Hz resolution).

6.0 RESULTS OF SPATIAL FILTERING EXPERIMENTS

This chapter describes the implementation of modal-space active damping using spatial filtering. The experimental and theoretical data to be presented in this chapter have not been presented previously.

The first test of this version of modal-space active damping was conducted on the cruciform beam structure. This structure was being used at the time for other research and could be used for a brief test of the control method (the beam-cable configuration had been replaced by the cruciform configuration). The first three modes were designated as controlled modes, with velocity sensors and dual force actuators at DOFs 9, 13, and 17 (refer to Figure 5 for DOF numbering). An analog control circuit was used to implement modal-space active damping with a design damping level of 0.1. The resulting closed-loop system demonstrated stable behavior with a significant damping increase observable. At this time, the PC-1000 digital array processor became available and was programmed to implement exactly the same control scheme. However, upon first application, an audible high frequency ringing developed and apparently precipitated the dynamic instability which was observed. The exact source of this behavior remains a mystery, but it was believed to involve high frequency noise and the delays involved in the array processor. The problem was eliminated when the design damping level was reduced to 0.03.

The driving point velocity frequency response function for DOF 17 is presented in Figure 15 for both the open-loop and closed-loop systems. These VFRFs resulted from sine chirp excitation, and the closed-loop data

(solid curve) is for the PC-1000 digital implementation of control with 0.03 damping. The closed-loop VFRF demonstrates the active damping applied to modes 1, 2, and 3, to the degree which was expected. Furthermore, large damping was also apparent in the residual modes (modes 4, 5, and 6 in the figure), as the open-loop resonances were all but eliminated. Transient decay measurements revealed a damping level of approximately 0.04 in modes 1 and 2, suggesting that the design damping was, in fact, achieved.

The primary test subject for the verification of control techniques was the hanging grid structure, since it was the most dynamically complex structure available. Accordingly, the majority of experimental testing and theoretical correlation was performed with this structure.

The controller design targeted five controlled modes, including modes 2 through 6, and employed five control force actuators at joints 1, 2, 4, 5, and 8 (see Figure 7). With the design damping set at 0.1, the control objectives and actuator configuration were identical to those for the case of control with spectral filtering. The new factors were the presence of the five velocity sensors, dual with the actuators, and the replacement of the troublesome spectral filters with the spatial filters.

It was at first thought that a number of sensors larger than the number of controlled modes would be desirable, since a larger number of sensors should provide a better estimate of modal response. Therefore, the number of sensors was initially set to 8, with additional sensors located at joints 3, 9, and 12, where no actuators were located. Inspection of the structure's first eight mode shapes led to this arrangement of sensors around the perimeter of the grillage of aluminum bars, which seemed to

avoid nodal regions as much as was possible. However, theoretical analysis of this configuration revealed unstable roots for the closed-loop structure-control system. The list of closed-loop system roots given in Table 4 demonstrates the residual mode instabilities which were predicted for this non-dual arrangement. Instabilities were also predicted by the theory for several other combinations of controlled mode sets and sensor locations, including configurations with only six or seven sensors. A stable case was not found until the number of sensors was reduced to five, where all sensors were dual with actuators.

Therefore, the controller configuration chosen to be tested consisted of the five dual actuator-sensor pairs at joints 1, 2, 4, 5, and 8. The feedback matrix which was designed to produce this control was calculated from Equation 23 and is presented in Table 5. Each column of this matrix corresponds to a sensor location and each row corresponds to an actuator location. For example, column 3 pertains to the sensor at joint 4 and row 1 pertains to the actuator at joint 1.

This configuration of modal-space active damping was implemented with the PC-1000 digital array processor. When the control system was activated, there was no apparent noise from the structure, nor any other evidence of instability, as there had been with the cruciform beam structure. The system appeared quite stable and clearly damped all low frequency vibrations rapidly. Closer aural inspection with one's ear extremely close to, but not touching, the grillage revealed a high-pitched noise which seemed to be comprised of several tones. This behavior did not exhibit itself at a level which could be measured and did not seem

to impair control system performance. The noise may have been caused by the discrete-time character of the controller's output signals.

Experimental measurements of the control system's performance consisted of forced response testing with both random-phased spectrum excitation and slow, incremental sine sweep testing. Random-phased excitation was used to generate broad-band frequency response functions for comparison of open- and closed-loop system behavior. The sine sweep tests were intended to generate narrow-band, high-resolution frequency responses for use with the curve-fit procedure to obtain experimentally measured values for damping and frequency. However, it turned out to be difficult to obtain curve-fit results for most of the closed-loop data due to the high damping levels which were present. This high damping probably violated many of the assumptions used in the available curve-fit algorithm, which was based on a viscous damping model presuming non-coupling modal damping. This curve-fit software, and all other data acquisition and analysis software was contained in the Vibration Analysis and Measurement Processor (VAMP), Version V5, obtained from Synergistic Technology, Incorporated. Open-loop damping values were measured with the curve-fit process and the values so obtained (listed in Table 6) were used in the theoretical model.

The theoretical analysis for this closed-loop system not only predicted stablity, but also indicated that the control would have beneficial spillover into the residual modes and provide significant amounts of active damping in these modes, in addition to the 0.1 damping applied to the five controlled modes. Table 6 lists theoretically predicted damping and frequency values for the open- and closed-loop

systems (the open-loop damping ratios are actually experimentally measured quantities, resulting from curve-fits). The closed-loop theoretical damping ratios indicate the strong control system performance, matching the design values for the controlled modes and significantly increasing the damping in all residual modes except modes 7 and 8. The high damping and concurrent modal coupling prevented all but a few closed-loop modal dampings from being measured with the curvefit procedure. Modes 3, 4, and 5 were all found to have experimental damping factors in excess of 0.1, however.

Figure 16 gives the experimentally measured driving point VFRF for excitation at joint 2 and the corresponding theoretical VFRF. The frequency range depicted is 0 to 10 Hz, spanning the first thirteen modes, where each mode is indicated with a numeral at the open-loop resonance peak. The closed-loop system, as indicated with the solid curve, can be seen to have greatly reduced response throughout the frequency range, including most of the residual modes. Mode 1, for example, receives substantial active damping, despite being omitted from the set of controlled modes. This result is in agreement with the theoretically predicted value of $\zeta_1 = 0.444$. Figure 17 gives the experimental and theoretical VFRFs for excitation at grid point 2 and velocity response measured at grid point 1. Both sets of data show evidence of good control system performance and excellent correlation between theoretical predictions and experimental data.

Closer examination of the FRFs indicates that not all residual modes were actively damped by the controller. As can be seen in Figure 16, the levels of response in modes 7 and 8 have not been significantly reduced

by the application of control, which suggests that these modes escaped most of the effects of this implementation of modal-space active damping. Vibrations in these modes were observed (visually) to continue in the central region of the aluminum grillage long after all other vibrations had been suppressed by the control system. This result is not surprising, since modes 7 and 8 are primarily top beam modes, with some motion in the center of the grillage, where there are no actuator-sensor pairs. An attempt to decrease the response in these modes, particularly mode 7, is detailed in Chapter 9.

The strong agreement between experimental and theoretical frequency responses does lend credence to the theoretical damping values of Table 6.

Figure 18 gives an experimental FRF for the frequency range 10 to 31 Hz, which shows some of the higher residual modes, including modes 14 through 22. This figure gives the driving point VFRF at joint 2. Mode 16 does not appear in the response due to a nodal region in the vicinity of joint 2. The spillover of active damping can be seen to extend through mode 21, with modes 14 and 15 being heavily damped. No data has been gathered for any modes higher than 31 Hz.

Table 4. System roots of grid with spatial filtering (non-dual)

Modal-Space Active Damping
(with 8 sensors and 5 actuators)
Closed-loop roots

Mode r	f_r(Hz)	ζ_r
1	0.584	.0108
2	0.860	.0904
3	1.361	.0976
4	3.270	.107
5	3.607	.108
6	5.022	.0975
7	5.485	.0013
8	5.654	.0010
9	5.760	.0474
10	7.970	-.0041
11	8.953	.0114
12	9.574	.101
13	*	
14	10.38	-.0587
15	13.27	.0038
16	20.56	.0040
17	25.10	.0131
18	27.00	.0058
19	29.14	.0069
20	30.62	.0051

* - indicates that mode 13 was replaced by two real roots, both positive, and therefore unstable

Table 5. Feedback matrix for modal-space control with spatial filtering

Controlled modes: 2 3 4 5 6
Control pairs located at joints: 1 2 4 5 8

$$[C^{ac}] = \begin{bmatrix} -0.0488 & 0.0381 & -0.0031 & 0.0443 & 0.0083 \\ 0.0381 & -0.0525 & 0.0010 & -0.0361 & -0.0109 \\ -0.0031 & 0.0010 & -0.0084 & 0.0013 & 0.0073 \\ 0.0443 & -0.0361 & 0.0013 & -0.0625 & -0.0128 \\ 0.0083 & -0.0109 & 0.0073 & -0.0129 & -0.0246 \end{bmatrix} \text{ lb-sec/in}$$

Table 6. System roots of grid with spatial filtering (dual)

	Modal-Space Active Damping			
	Open-loop		Closed-loop	
Mode r	f_r(Hz)	ζ_r	f_r(Hz)	ζ_r
1	0.581	.0443	0.617	.444
2	0.870	.0287	0.838	.098
3	1.349	.0281	1.336	.127
4	3.190	.0116	3.213	.110
5	3.488	.0060	3.570	.0990
6	4.850	.0065	4.948	.0885
7	5.483	.0025	5.501	.0051
8	5.645	.0022	5.653	.0030
9	5.952	.0043	6.505	.118
10	7.898	.0033	7.908	.0273
11	8.182	.0041	8.472	.373
12	9.006	.0041	8.506	.0471
13	9.457	.0018	9.159	.0209
14	11.20	.0030	10.22	.0409
15	12.87	.0020	12.74	.0147
16	20.56	.0015	20.56	.0015
17	24.09	.0013	24.05	.0057
18	26.37	.0011	26.37	.0023
19	28.23	.0013	28.23	.0022
20	29.81	.0012	29.79	.0037

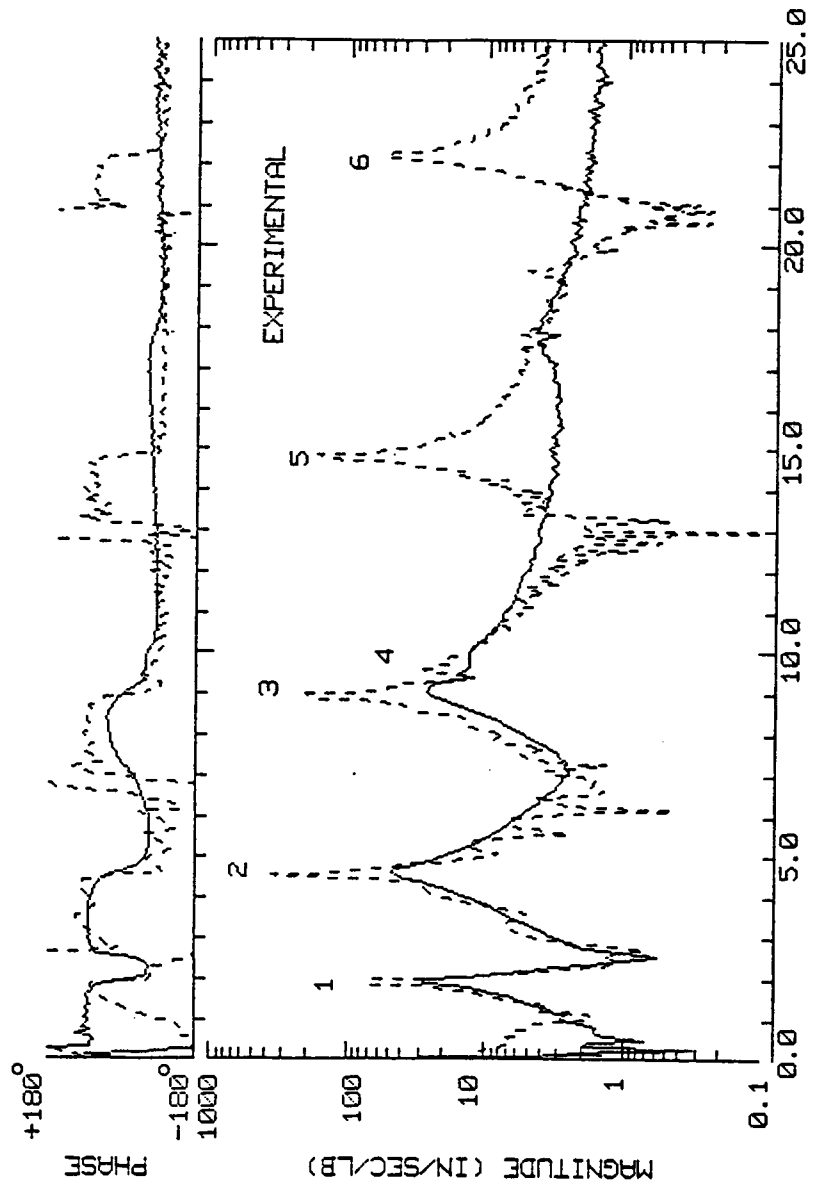

Figure 15. VFRF of cruciform beam with spatial filtering: Experimental VFRF with modal-space active damping; open-loop (broken) and closed-loop (solid); 0.025 Hz resolution.

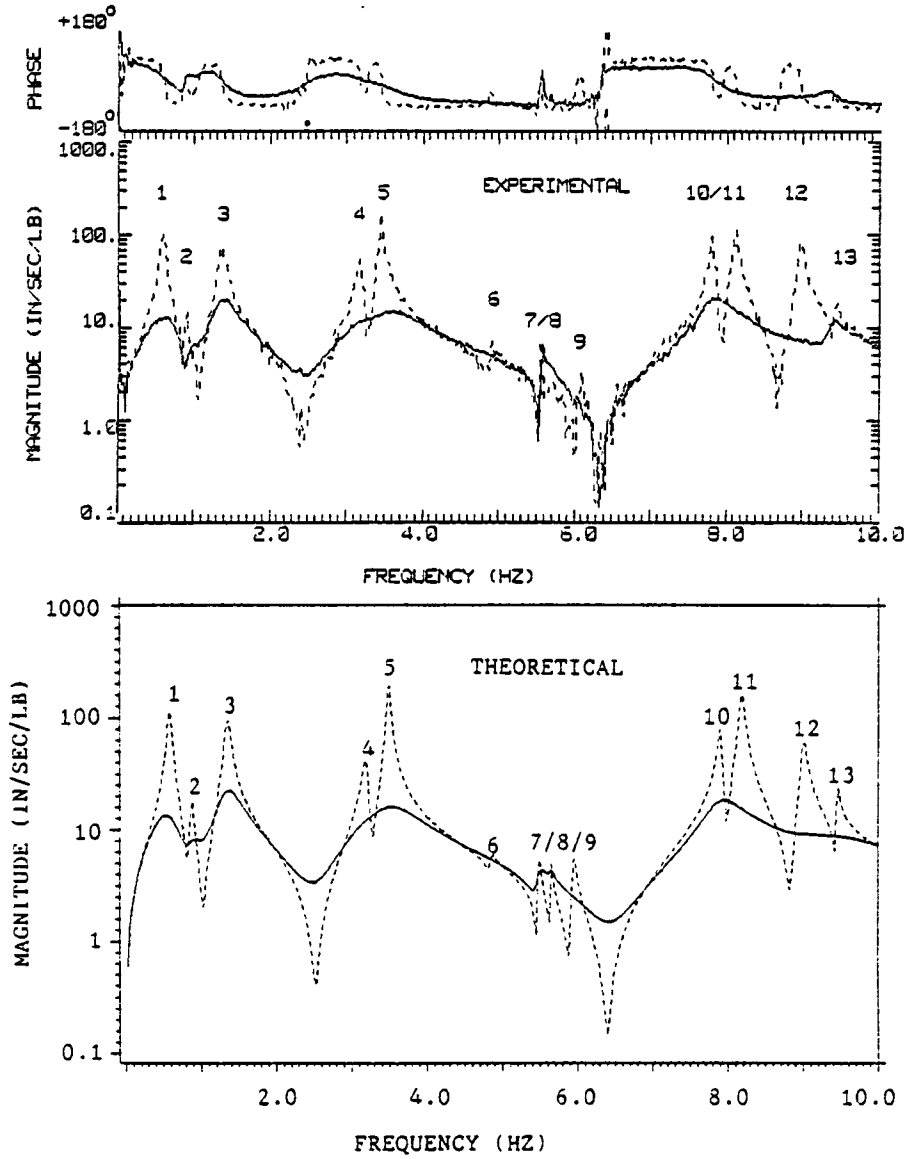

Figure 16. VFRF(2,2) of grid with spatial filtering approach: Solid curves are for closed-loop with modal-space active damping (0.025 Hz resolution).

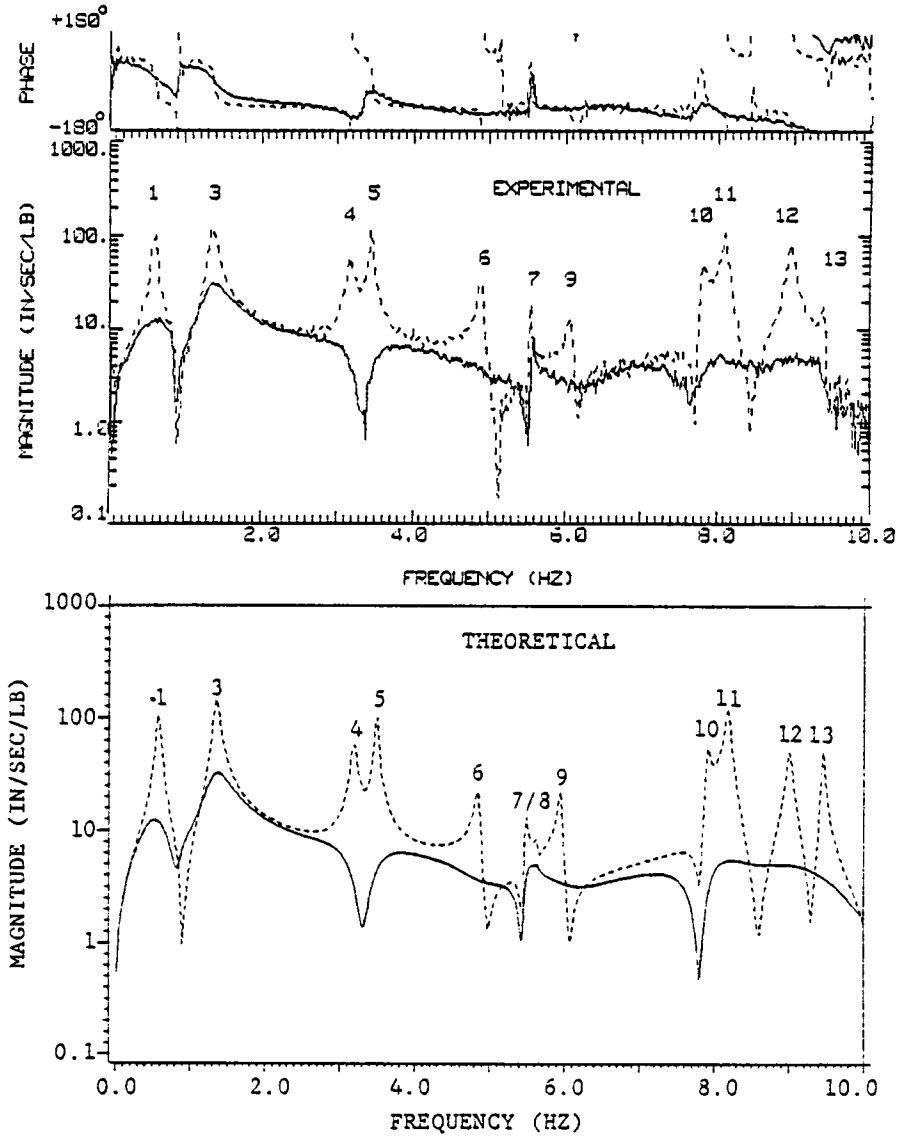

Figure 17. VFRF(1,2) of grid with spatial filtering approach: Solid curves are for closed-loop with modal-space active damping (0.025 Hz resolution).

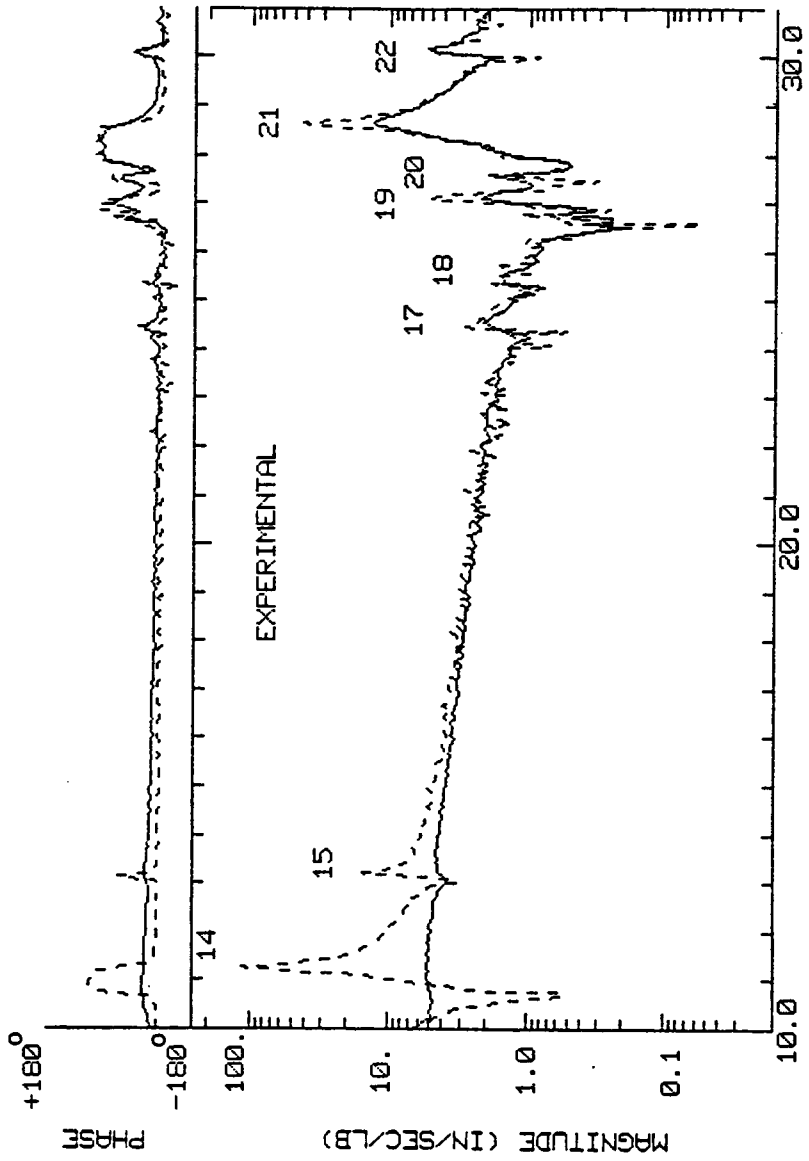

Figure 18. VFRF(2,2) of hanging grid for 10 to 31 Hz: Experimental data only; solid curve is for closed-loop data (0.075 Hz resolution).

7.0 RESULTS OF DIRECT RATE FEEDBACK EXPERIMENTS

Optimized rate feedback damping (see Section 2.4) was implemented on the hanging grid structure in an attempt to match the performance of modal-space active damping using a simpler control design. In the present study, this form of rate feedback damping employed a set of dual sensor-actuator pairs which acted simply as physical dashpots (or viscous dampers). This approach leads to a diagonal feedback matrix with no communication between non-dual sensors and actuators. Preston and Lin[15] performed an optimization of feedback with a dual configuration, but used a full (non-diagonal) feedback matrix. That would produce a control form which lies somewhere in between the direct rate feedback and modal-space active damping approaches used in this research.

The objectives of the present implementation of rate feedback active damping were identical to those for the modal-space active damping implementation discussed earlier (Chapter 6). Modes 2 through 6 were again targeted for 10% damping ($\zeta_s^c = 0.10$). The same sensor-actuator locations were used: at joints 1, 2, 4, 5, and 8. With these parameters, the linearized optimization procedure resulted in a feedback matrix of

$$[DF] = \text{diag}\ (0.0,\ 0.0,\ 0.0080,\ 0.0401,\ 0.0635)\ \text{lb-sec/in.}$$

The numbers in this matrix indicate the damping constants which were required of the sensor-actuator pairs at joints 1, 2, 4, 5, and 8, in order. The null gains indicated in this matrix show that the sensor-actuator pairs at joints 1 and 2 were not required in order to provide an active damping level of 0.10 in modes 2 through 6.

The theoretically predicted frequencies and damping ratios for the system with optimized rate feedback are listed in Table 7. The values given in this table indicate that this control method accomplishes the design objectives for the controlled modes and also has beneficial spillover into residual modes. The spillover damping has a decreasing effect with increasing frequency, but does extend through mode 15. Mode 1 again gets substantial damping (0.233), but modes 7 and 8 are not significantly damped by this control method, as had been the case for modal-space active damping. Comparison of Table 7 with Table 6 reveals that the direct rate feedback approach produced generally less spillover damping than did modal-space active damping. However, the direct rate feedback actually provided more damping in the controlled modes.

Figure 19 presents both measured and calculated VFRFs in the 0 to 10 Hz range for excitation and measurement at joint 2. The closed-loop data (solid curves) superimposed on the open-loop frequency response, shows the effects of applying optimized rate feedback to the hanging grid structure. The experimental data was generated using random-phased spectrum excitation. The theoretical and experimental responses appear well correlated and are consistent with the calculated roots. The response in controlled modes, and mode 1, was greatly reduced, as was the response in residual modes. The sharp peaks in modes 7 and 8 demonstrate the lack of damping in these modes. Comparison of this figure with Figure 16 suggests that the modal-space approach damped residual modes more heavily than did the rate feedback approach. Controlled mode response appeared comparable in the two cases. The experimental VFRFs for higher frequencies (10 to 31 Hz) are shown in Figure 20. Modes 14

and 15 had substantially reduced response with rate feedback applied, but higher modes received little or no active damping.

Table 7. System roots of hanging grid with optimized rate feedback

	Optimized Rate Feedback Damping			
	Open-loop		Closed-loop	
Mode r	f_r(Hz)	ζ_r	f_r(Hz)	ζ_r
1	0.581	.0443	0.716	.233
2	0.870	.0287	0.806	.549
3	1.349	.0281	1.236	.184
4	3.190	.0116	3.205	.117
5	3.488	.0060	3.539	.105
6	4.850	.0065	4.735	.115
7	5.483	.0025	5.483	.0044
8	5.645	.0022	5.644	.0034
9	5.952	.0043	5.914	.0321
10	7.898	.0033	7.903	.0186
11	8.182	.0041	8.178	.0433
12	9.006	.0041	8.860	.0328
13	9.457	.0018	9.422	.0139
14	11.20	.0030	11.11	.0324
15	12.87	.0020	12.81	.0171
16	20.56	.0015	20.56	.0015
17	24.09	.0013	24.09	.0030
18	26.37	.0011	26.36	.0030
19	28.23	.0013	28.23	.0027
20	29.81	.0012	29.81	.0019

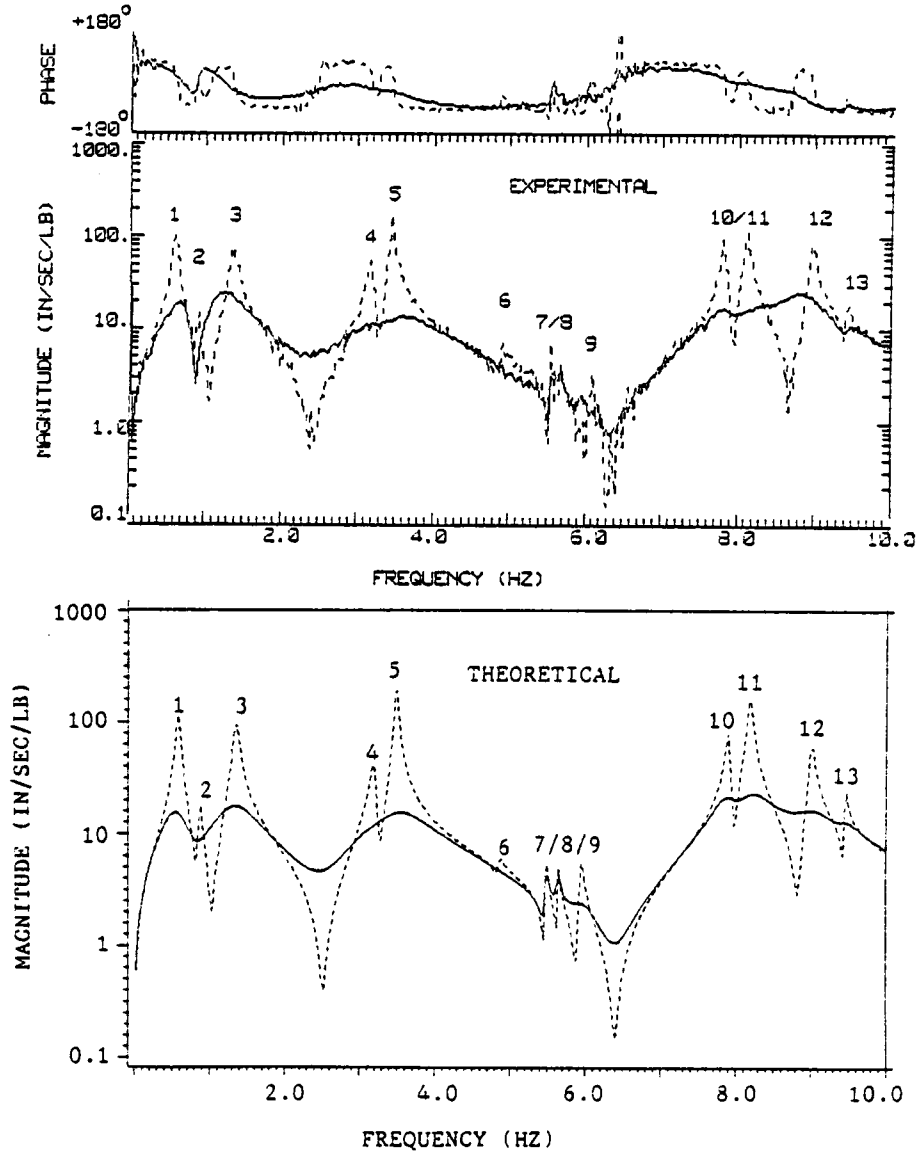

Figure 19. VFRF(2,2) of hanging grid with optimized rate feedback: Solid curves give closed-loop response (0.025 Hz resolution).

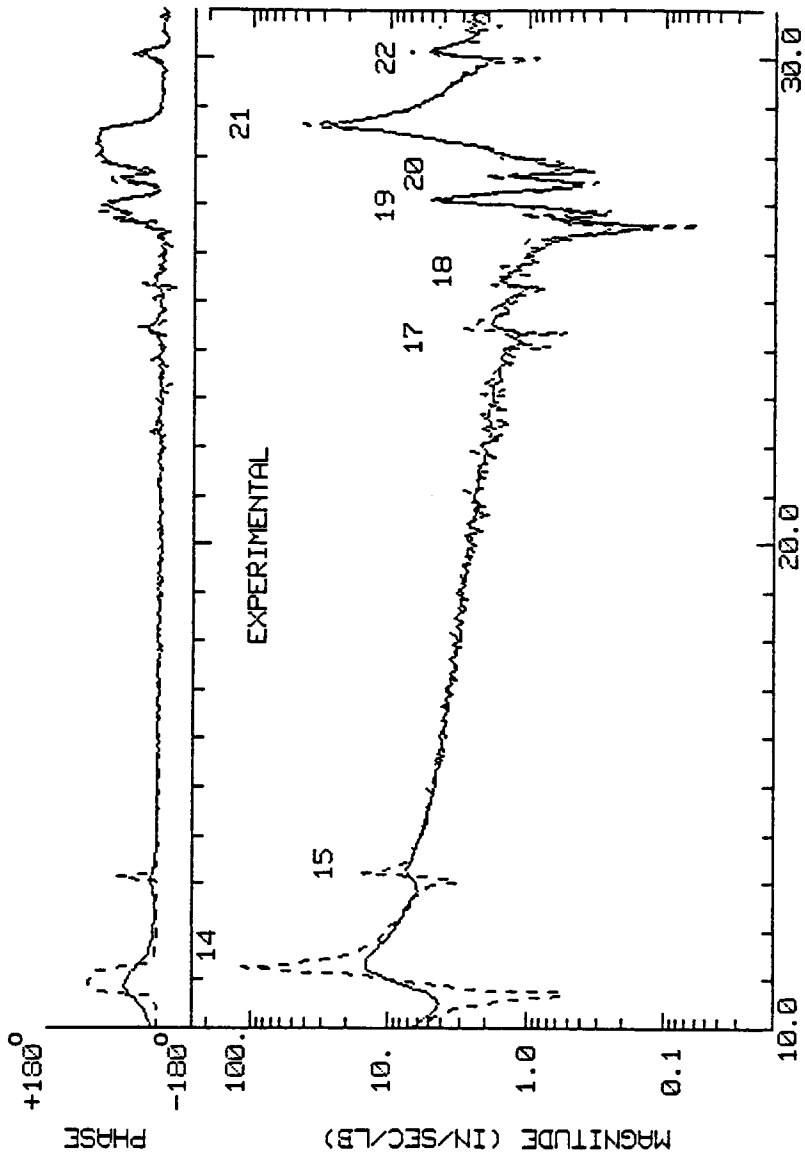

Figure 20. VFRF(2,2) of hanging grid for 10 to 31 Hz: Experimental data only; solid curve is for closed-loop response (0.075 Hz resolution).

8.0 RESULTS OF PSEUDO-INVERSE CONTROL EXPERIMENTS

The pseudo-inverse approach to active damping of a greater number of modes than the number of actuators (see Section 2.5) was implemented in two versions on the hanging grid structure. Equation 31 describes the computation of the contol matrix, which relies on matrix pseudo-inverses. This form of active damping will therefore be referred to in this study as pseudo-inverse control, for the sake of brevity. The two versions of this approach consisted of six mode control and ten mode control. Each was implemented with the same set of five dual sensor-actuator pairs which were used in modal-space active damping and direct rate feedback damping; the locations remained at joints 1, 2, 4, 5, and 8. All controlled modes were targeted for 10% damping ($\zeta_s^c = 0.10$). The six mode control version included mode 1 in the controlled mode set (in addition to modes 2 through 6). These parameters produced the first control matrix shown in Table 8. With modes 1, 9, 10, 11, and 12 added to the original set of controlled modes, the ten mode control version was implemented with the second matrix shown in Table 8. Modes 7 and 8 were not designated as controlled modes because they were primarily top beam modes of the structure which could not be successfully damped by actuators located on the grillage portion of the structure. This had been made obvious by observations of previous control systems' performance relative to these modes, and by some preliminary numerical experiments. The feedback terms in Table 8 indicate a general decrease in gains as more modes were to be controlled.

The theoretical closed-loop roots for both the six and ten mode control versions are listed in Table 9. In both cases, damping factors

were generally lower than for the basic (five mode) modal-space active damping (see Table 6) Performance in modes 2 through 6 was not seriously impaired, but the damping in new controlled modes was less than it had been when those modes were residual modes, damped only by beneficial spillover.

The decreased damping was also apparent in frequency response data. Figure 21 shows the six mode control closed-loop VFRF superimposed on the open-loop data and the five mode modal-space active damping data. The figure is for the driving point VFRF at joint 2 and uses solid lines for the six mode control and broken lines for the five mode control and the open-loop data. Figure 22 shows the corresponding data for ten mode control. In both instances, the closed-loop resonant response was generally higher for pseudo-inverse control than for the basic five mode control. The effect is especially pronounced in mode 1, which received much less active damping as a controlled mode than it did as a residual mode. As before, modes 7 and 8 received essentially no damping from this control technique. Modes 11 and 12 received greater damping as residual modes in six mode control than as controlled modes in ten mode control, as evidenced by comparison of Figure 21 and Figure 22 and by the list of roots given in Table 9. The frequency responses again show reasonably good agreement between experiment and theory.

These results seem to suggest that overall system performance can be degraded by attempting to extend active damping to a greater number of controlled modes than the number of actuators used.

Table 8. Control matrices for 6- and 10- mode control of grid

6 MODE CONTROL
Controlled modes: 1 2 3 4 5 6
Control pairs located at joints: 1 2 4 5 8

$$[C^{ac}] = \begin{bmatrix} -0.0451 & 0.0289 & -0.0046 & 0.0371 & 0.0041 \\ 0.0289 & -0.0313 & 0.0040 & -0.0186 & -0.0011 \\ -0.0046 & 0.0040 & -0.0080 & 0.0041 & 0.0087 \\ 0.0371 & -0.0186 & 0.0041 & -0.0487 & -0.0048 \\ 0.0041 & -0.0011 & 0.0087 & -0.0048 & -0.0202 \end{bmatrix} \text{ lb-sec/in}$$

10 MODE CONTROL
Controlled modes: 1 2 3 4 5 6 9 10 11 12
Control pairs located at joints: 1 2 4 5 8

$$[C^{ac}] = \begin{bmatrix} -0.0189 & 0.0116 & 0.00014 & 0.0135 & 0.00057 \\ 0.0116 & -0.0240 & 0.00075 & -0.0056 & -0.0015 \\ 0.00014 & 0.00075 & -0.0075 & 0.00026 & 0.0051 \\ 0.0135 & -0.0056 & 0.00026 & -0.0273 & -0.00033 \\ 0.00057 & -0.0015 & 0.0051 & -0.00033 & -0.0188 \end{bmatrix} \text{ lb-sec/in}$$

Table 9. System roots of hanging grid with pseudo-inverse control

Control of More Modes Than Actuators

	Open-loop		6 Mode Control		10 Mode Control	
Mode r	f_r(Hz)	ζ_r	f_r(Hz)	ζ_r	f_r(Hz)	ζ_r
1	0.581	.0443	0.583	.129	0.596	.230
2	0.870	.0287	0.870	.0795	0.854	.123
3	1.349	.0281	1.345	.106	1.342	.128
4	3.190	.0116	3.214	.111	3.206	.0900
5	3.488	.0060	3.558	.0998	3.499	.0730
6	4.850	.0065	4.967	.0908	4.871	.0749
7	5.483	.0025	5.502	.0054	5.491	.0054
8	5.645	.0022	5.652	.0031	5.649	.0033
9	5.952	.0043	6.256	.136	5.969	.0524
10	7.898	.0033	7.916	.0281	7.898	.0216
11	8.182	.0041	8.401	.0547	8.195	.0424
12	9.006	.0041	8.827	.189	9.083	.0398
13	9.457	.0018	9.163	.0228	9.372	.0286
14	11.20	.0030	10.40	.0529	11.03	.0523
15	12.87	.0020	12.76	.0153	12.81	.0147
16	20.56	.0015	20.56	.0015	20.56	.0015
17	24.09	.0013	24.06	.0058	24.08	.0035
18	26.37	.0011	26.37	.0023	26.37	.0021
19	28.23	.0013	28.23	.0021	28.23	.0020
20	29.81	.0012	29.79	.0037	29.81	.0023

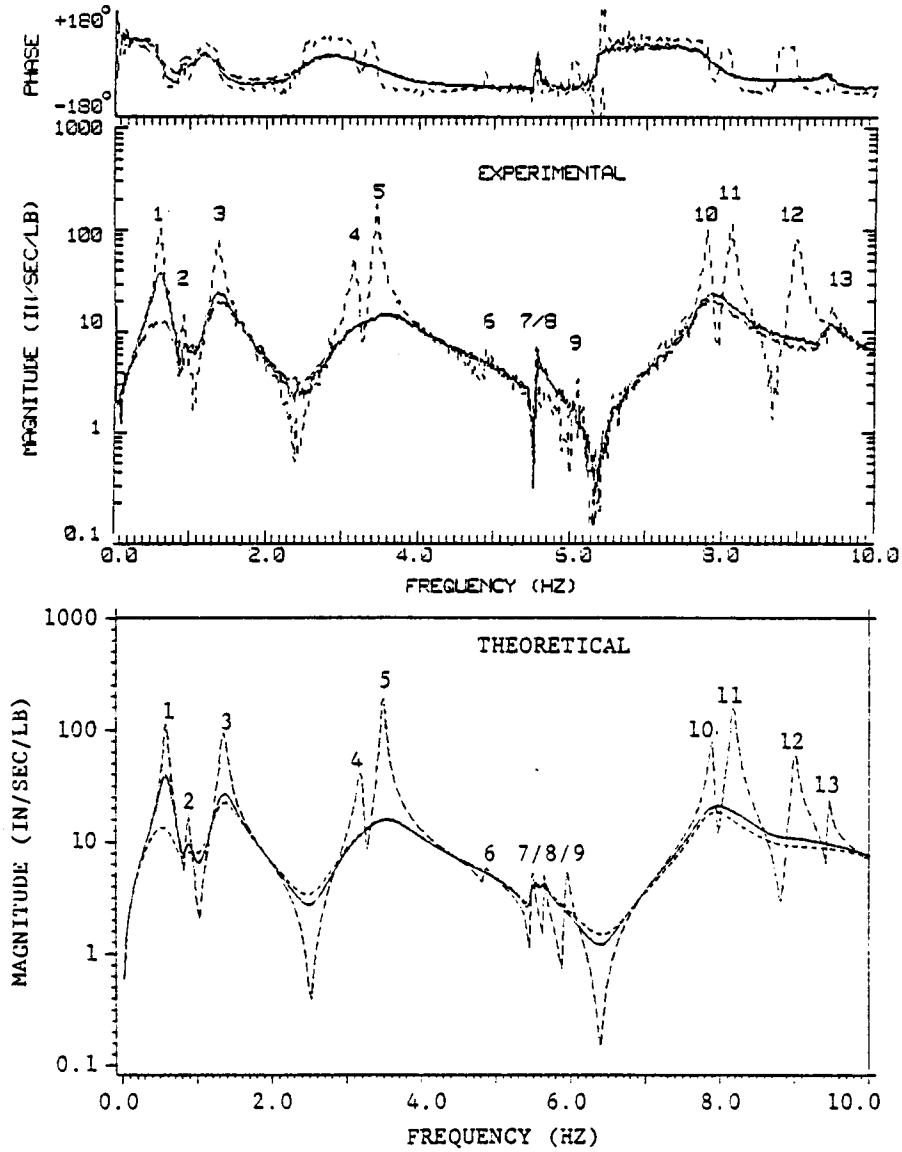

Figure 21. VFRF(2,2) of hanging grid for six controlled modes: Solid curves are for 6 mode control; broken lines indicate data for open-loop and 5 mode control (0.025 Hz resolution).

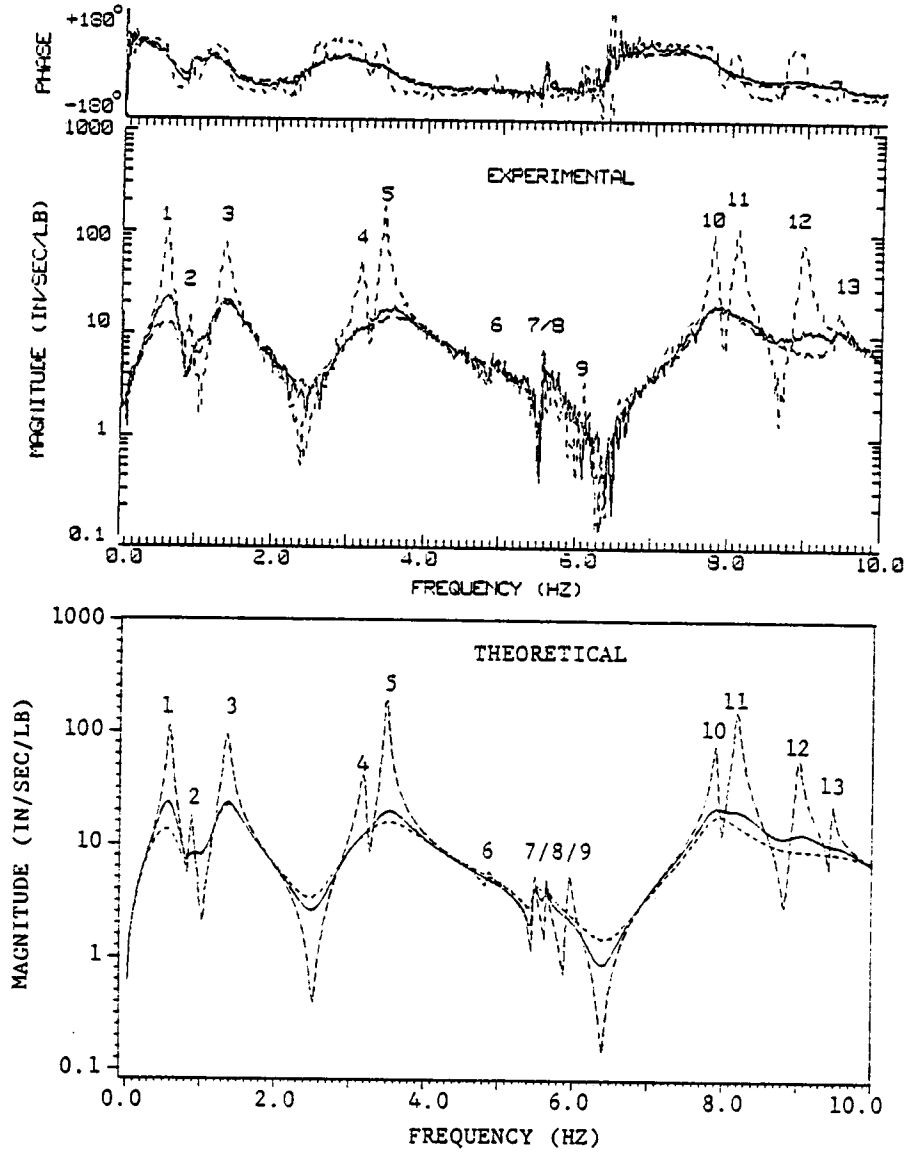

Figure 22. VFRF(2,2) of hanging grid for ten controlled modes: Solid curves are for 10 mode control; broken lines indicate data for open-loop and 5 mode control (0.025 Hz resolution).

9.0 RESULTS OF HYBRID CONTROL EXPERIMENTS

As discussed in previous chapters on experimental results, modes 7 and 8 of the hanging grid structure were left unaffected by the application of the various control forms. The lack of active damping on these modes resulted in a lingering vibration (at approximately 5.6 Hz) in the central region of the grillage, which continued after all other vibrations had been suppressed by the active damping system.

It was hypothesized that a simple direct rate feedback controller (used in addition to the basic modal-space active damping system) placed at joint 6 could decrease the amplitude of motion of modes 7 and 8 in the central region of the grillage, even if it could not provide high damping in these modes. The large mass of the steel top beam, which predominated in these two modes, apparently made it impossible to increase the modal dampings substantially with actuators acting through the light, flexible grillage. The actuators located around the perimeter of the grillage had been observed to create nodal regions around the edges of the grillage, so that all residual motions were concentrated in the central region. Therefore, an additional rate feedback controller placed within that region might be able to decrease the amplitude of this motion.

To implement this form of hybrid control, a dual sensor-actuator pair had to be placed on the structure. Therefore, two coils (one for a sensor, one for an actuator) were attached to the structure at joint 6. At the same time, the sensor coils located at joints 3, 9, and 12 (which were never used) were removed from the structure. This redistribution of coil masses represented enough of a structural modification to

necessitate a new theoretical dynamic analysis of the structure. The calculated natural frequencies, which changed only slightly due to the small mass changes, are listed in Table 10. The open-loop modal dampings listed in this table were assumed not to have changed from their previous values.

The control matrix for modal-space active damping (with spatial filtering) was recalculated for the new natural frequencies and mode shapes. The matrix for $\zeta_s^c = 0.10$ in modes 2 through 6 with dual sensor-actuator pairs at joints 1, 2, 4, 5, and 8 is shown in Table 11. Use of the new control matrix resulted in the calculated closed-loop roots listed in Table 10. The values in this table are not very different from the roots for modal-space active damping with the original set of coil locations. In particular, modes 7 and 8 were still not actively damped.

Figure 23 shows open- and closed-loop (modal-space active damping only) VFRFs for measurement and excitation at joint 2. This data is very similar to the data from before the structure was modified (see Figure 16). Figure 24 shows the VFRFs for the same case, but for the response at joint 6 (and excitation still at joint 2). This figure clearly shows the sharp closed-loop peak in mode 7. This is the specific response that the hybrid control would be aimed at reducing. Experimental and theoretical data show good correlation, except that the mode shapes for modes 10, 12, and 13 may be in error, especially for response at joint 6.

Rate feedback control was implemented at joint 6 using an analog circuit for feedback from the velocity sensor to the force actuator. A sixth controlled-current power amplifier was not available, so an older,

less-efficient power amplifier design was used. This permitted some additional damping due to the motion of the actuator coil, but this was accounted for in the calculation of the feedback gain. Details on the power amplifier design and allowance for the additional damping can be found in Reference 19.

The damping constant required of this additional controller pair was not determined through a formal optimization procedure, but through calculation of a locus of roots. A value of 0.15 lb-sec/in was found to give the maximum damping increase in most modes. Table 11 indicates how this control was implemented in the theoretical model, with row and column 6 of the matrix [F] corresponding to the feedback between the sensor and actuator at joint 6.

The additional feedback control, acting in conjunction with modal-space active damping, resulted in the theoretical roots shown in the last column of Table 10. These roots demonstrate an increased damping in most modes over the modal-space damping results, including a threefold increase in mode 7. Mode 1 was nearly critically damped by the hybrid control. The damping in mode 2 was decreased slightly by any feedback at joint 6. Modes 16 and above were still not significantly damped.

Figure 25 and Figure 26 show the measured and calculated VFRFs for the closed-loop system with hybrid control (solid curves). Figure 25 gives the driving point frequency response, VFRF(2,2). Figure 26 gives VFRF(6,2) which demonstrates the decrease in the amplitude of response in mode 7, even though the mode did not receive a large amount of damping. In this case (for a non-driving point frequency response), a decreased

peak amplitude is indicative of a closed-loop mode shape change and some increase in damping.

Table 10. System roots of modified hanging grid structure

Mode r	Open-loop		Modal-Space Control Alone		Hybrid Control	
	f_r(Hz)	ζ_r	f_r(Hz)	ζ_r	f_r(Hz)	ζ_r
1	0.581	.0443	0.619	.444	0.802	.911
2	0.874	.0287	0.841	.0984	0.872	.095
3	1.343	.0281	1.330	.127	1.123	.380
4	3.203	.0116	3.233	.110	3.264	.120
5	3.499	.0060	3.585	.0956	3.581	.246
6	4.863	.0065	4.942	.0871	4.788	.242
7	5.477	.0025	5.487	.0041	5.450	.0137
8	5.645	.0022	5.653	.0028	5.653	.0037
9	6.035	.0043	6.939	.0982	6.488	.168
10	7.792	.0033	7.901	.0308	7.801	.210
11	8.169	.0041	8.435	.0529	8.045	.0433
12	9.234	.0041	8.107	.484	8.903	.300
13	9.735	.0018	9.487	.0192	9.506	.0205
14	11.33	.0030	10.39	.0327	9.860	.0606
15	12.92	.0020	12.81	.0138	12.66	.0254
16	20.56	.0015	20.56	.0015	20.56	.0015
17	24.22	.0013	24.17	.0062	24.18	.0065
18	26.14	.0011	26.14	.0023	26.14	.0023
19	28.27	.0013	28.27	.0022	28.23	.0028
20	29.78	.0012	29.77	.0026	29.75	.0041

Table 11. Control matrices for hybrid control

MODAL-SPACE ACTIVE DAMPING
Controlled modes: 2 3 4 5 6
Control pairs located at joints: 1 2 4 5 8

$$[C^{ac}] = \begin{bmatrix} -0.0559 & 0.0438 & -0.0034 & 0.0518 & 0.0087 \\ 0.0438 & -0.0566 & 0.0015 & -0.0425 & -0.0110 \\ -0.0034 & 0.0015 & -0.0080 & 0.0015 & 0.0068 \\ 0.0518 & -0.0425 & 0.0015 & -0.0705 & -0.0128 \\ 0.0087 & -0.0110 & 0.0068 & -0.0128 & -0.0232 \end{bmatrix} \text{ lb-sec/in}$$

HYBRID CONTROL
Rate feedback control pair located at joint 6
G = -0.15 lb-sec/in

$$[F] = \begin{bmatrix} [C^{ac}] & [0] \\ [0] & G \end{bmatrix}$$

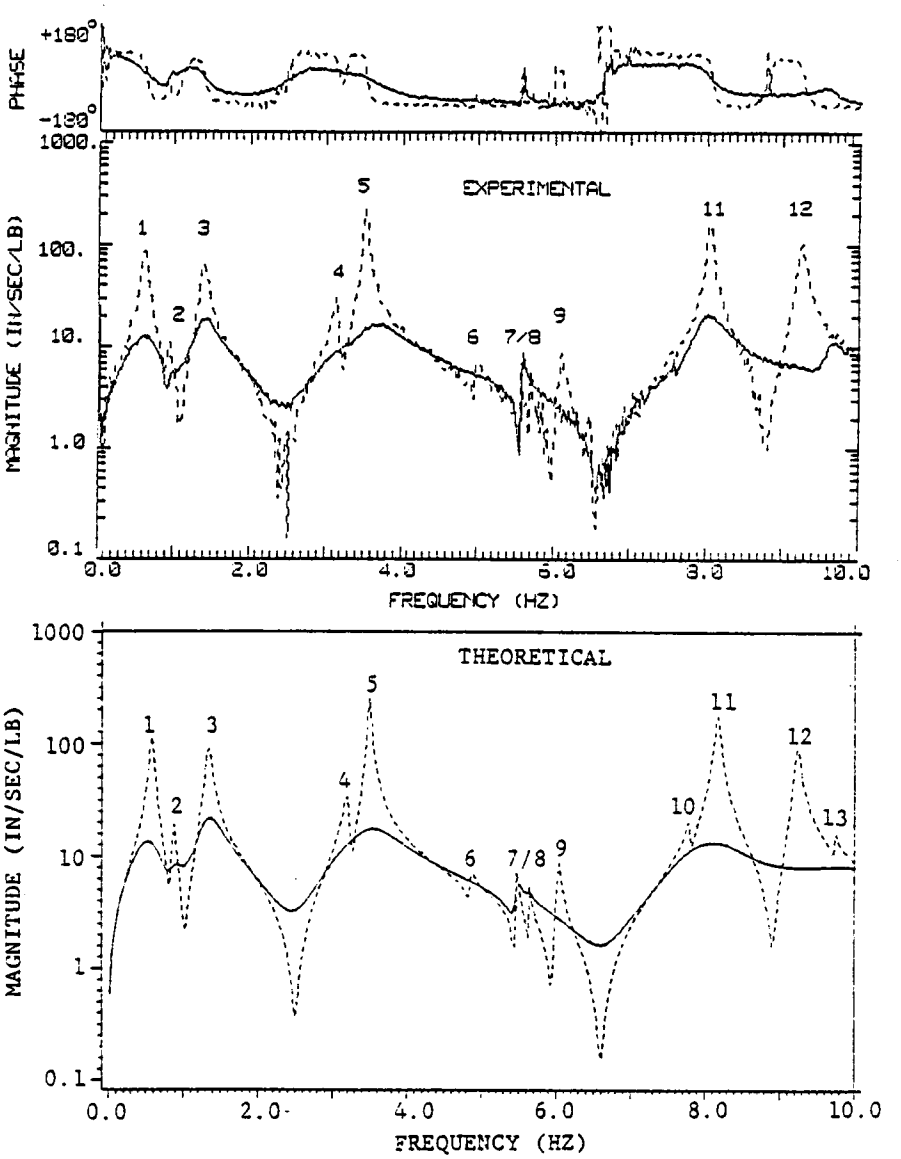

Figure 23. VFRF(2,2) of hanging grid with modal-space active damping: Data is for modified structure; solid curve is for modal-space active damping only (0.025 Hz resolution).

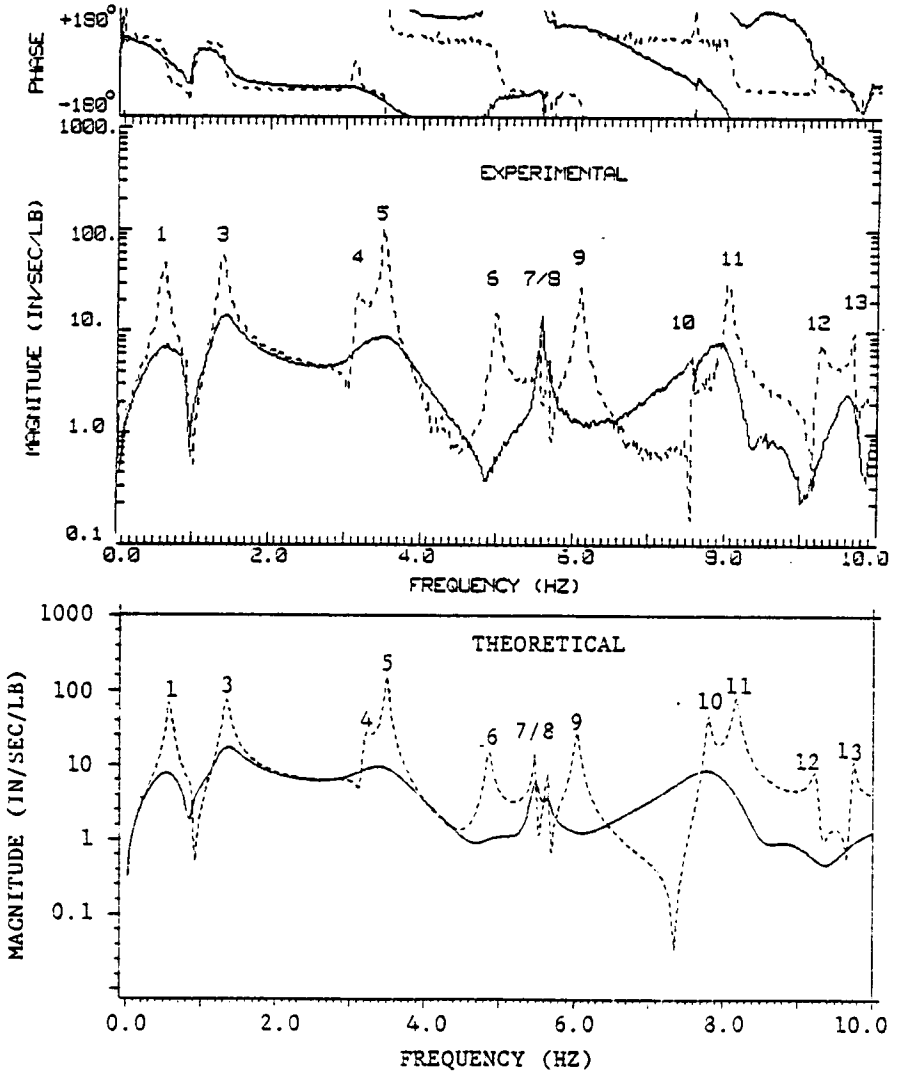

Figure 24. VFRF(6,2) of hanging grid with modal-space active damping: Data is for modified structure; solid curve is for modal-space active damping only (0.025 Hz resolution).

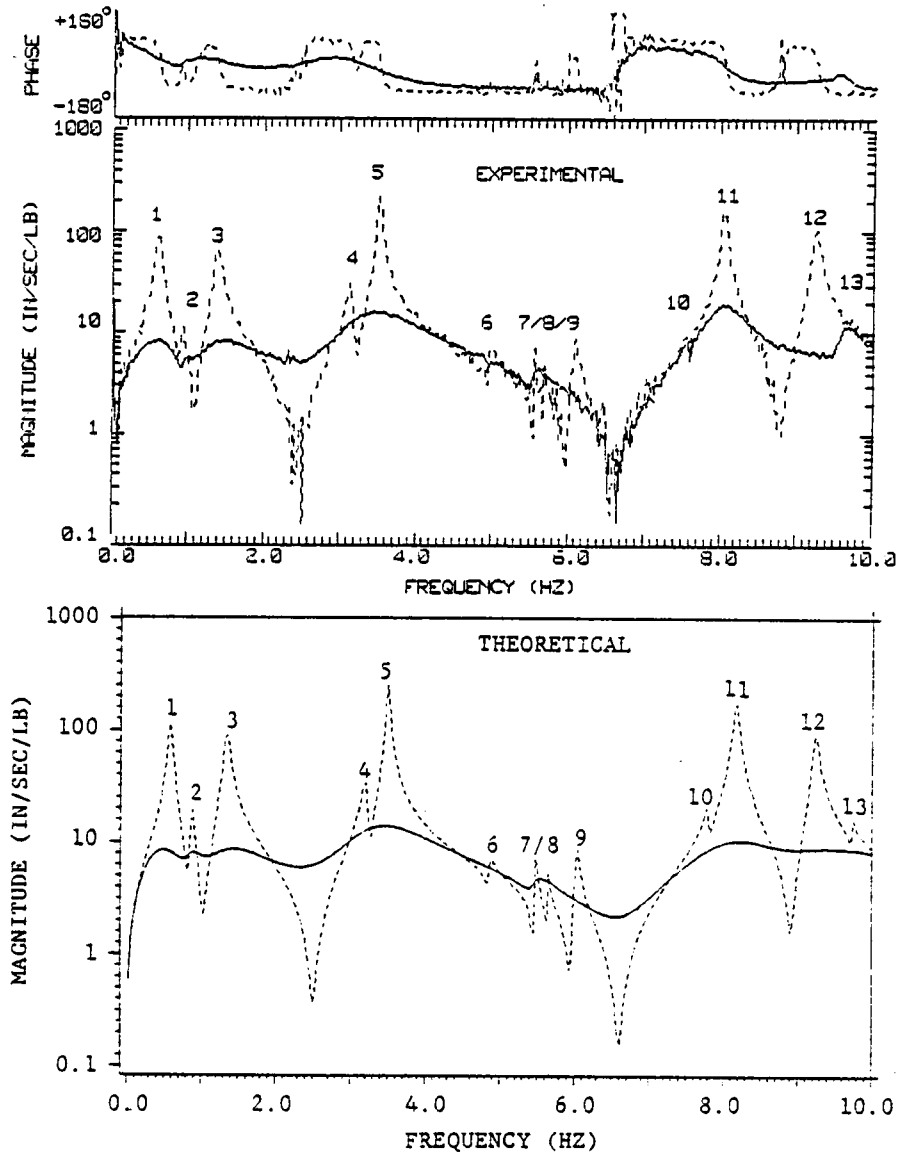

Figure 25. VFRF(2,2) of hanging grid with hybrid control: Data is for modified structure; solid curve is for hybrid control; dashed curve for open-loop (0.025 Hz resolution).

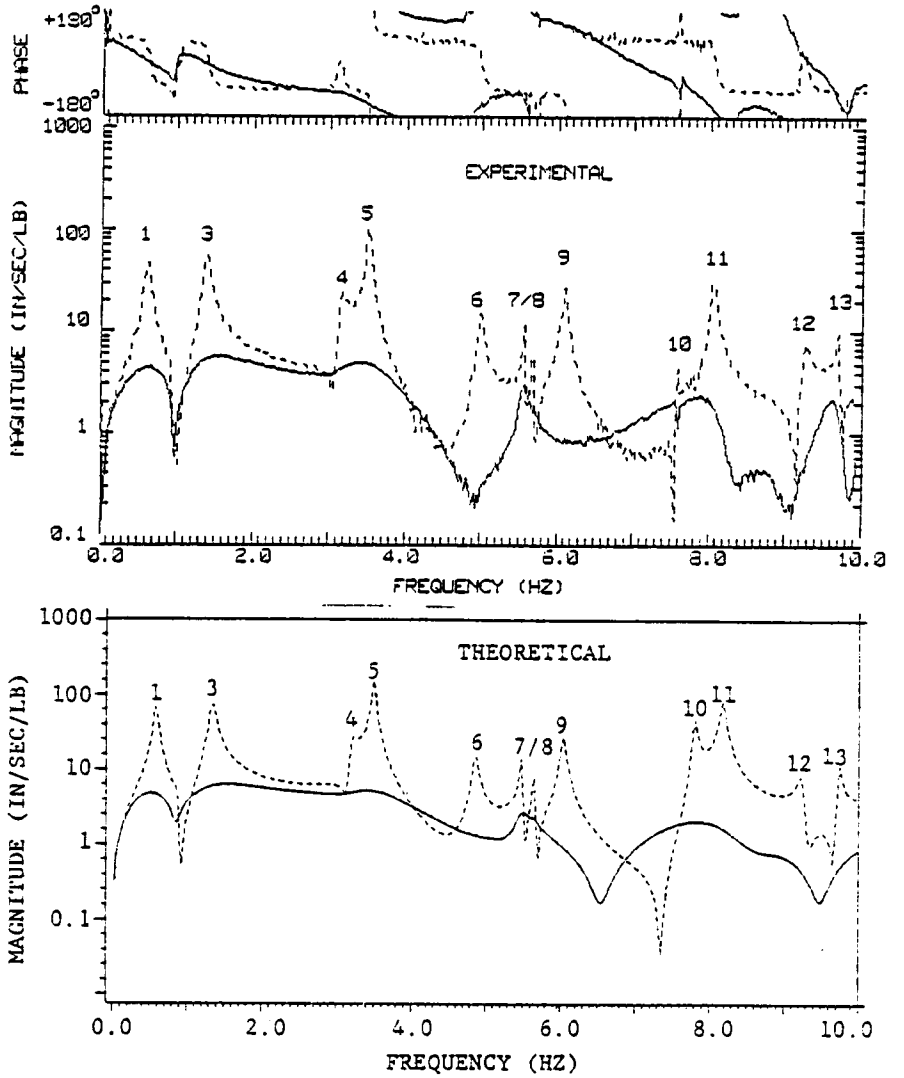

Figure 26. VFRF(6,2) of hanging grid with hybrid control: Data is for modified structure; solid curve is for hybrid control; dashed curve for open-loop (0.025 Hz resolution).

10.0 SUMMARY AND CONCLUSIONS

Several related forms of active damping were implemented experimentally and theoretically, primarily on the hanging grid structure. Calculated frequency response functions were generally in good agreement with experimental measurements. Since frequency response and eigenanalysis were based on the same model and the same mathematical analysis, the theoretical-experimental correlation tends to validate the theoretically calculated system roots which serve to quantify active damping performance.

The spectral filtering approach to modal-space active damping was previously found to be unsatisfactory. Design damping values could not generally be achieved, since performance was more dependent on filter design than on the target damping level. The coupling between the dynamic filters and the dynamics of the structure seriously impaired control system performance and was capable of precipitating dynamic instability.

The spatial filtering (or static observation) approach to modal estimation permitted the elimination of the spectral filters and created a reliable, stable form of modal-space active damping. This form of control was shown to be stable whenever a dual configuration of sensors and actuators was used. Controlled modes were observed to receive a substantial percentage of the desired active damping, and control spillover was beneficial, adding damping to many of the residual modes and leaving the remainder unaffected. Modal-space active damping was extended to the control of a greater number of modes than available actuators through the use of matrix pseudo-inverses. Such additional

design effort was not rewarded with improved performance, as the additional modes brought into the controlled mode set were not as heavily damped as they had been in the original modal-space active damping system (with spatial filtering).

Direct rate feedback damping with optimized gains was implemented and compared to the modal-space approach, as design objectives were used which were equivalent to those used in the basic modal-space active damping system. Damping in controlled modes was actually higher for optimized rate feedback, but residual mode damping was lower. Also, comparable controlled mode performance was achieved with fewer actuators, as the specific case presented in this study had only three active pairs out of the five available sensor-actuator pairs and yet controlled five modes.

A hybrid control form which combined modal-space active damping with simple direct rate feedback was implemented. The application was intended to reduce the response of a residual mode which was not actively damped by the modal-space approach alone. The resulting control was effective in reducing the response of this mode and providing additional damping in most of the other modes which were examined.

It should be noted that while the various control forms were implemented successfully, simple actuators and sensors were used which were not structure-borne. The complicated dynamics of structure-borne actuators and sensors (which will have to be used in any realistic applications) may impair the performance of active damping systems. Studies of such effects are left for further research. Nevertheless, this study was successful in evaluating and comparing several basic control

laws and accumulating data on the interaction of structures and basic control systems.

REFERENCES

1. G. S. Nurre, R. S. Ryan, H. N. Scofield, and J. L. Sims, "Dynamics and Control of Large Space Structures," Journal of Guidance, Control, and Dynamics, Vol. 7, No. 5, September-October, 1984, pp. 514-526.

2. J. N. Aubrun, M. J. Ratner, and M. G. Lyons, "Structural Control for a Circular Plate," Journal of Guidance, Control, and Dynamics, Vol. 7, No. 5, September-October, 1984, pp. 535-545.

3. D. B. Schaechter and D. B. Eldred, "Experimental Demonstration of the Control of Flexible Structures," Journal of Guidance, Control, and Dynamics, Vol. 7, No. 5, September-October, 1984, pp. 527-534.

4. R. D. Bauldry, J. A. Breakwell, G. J. Chambers, K. F. Johnson, N. C. Nguyen, and D. B. Schaechter, "A Hardware Demonstration of Control for a Flexible Offset-Feed Antenna," The Journal of the Astronautical Sciences, Vol. 31, No. 3, July-September, 1983, pp.455-470.

5. L. Meirovitch, H. Baruh, R. C. Montgomery, and J. P. Williams, "Nonlinear Natural Control of an Experimental Beam," Journal of Guidance, Control, and Dynamics, Vol. 7, No. 4, July-August, 1984, pp. 437-442.

6. G. R. Skidmore, "A Study of Modal-Space Control of a Beam-Cable Structure: Experiment and Theory," M. S. Thesis, Virginia Polytechnic Institute and State University, 1983.

7. G. R. Skidmore and W. L. Hallauer Jr., "Modal-Space Active Damping of a Beam-Cable Structure: Theory and Experiment," Journal of Sound and Vibration, scheduled for publication in 1985.

8. W. L. Hallauer Jr., G. R. Skidmore, and R. N. Gehling, "Modal-Space Active Damping of a Plane Grid Structure: Theory and Experiment," Journal of Guidance, Control, and Dynamics, scheduled for publication in the May-June, 1985 edition.

9. J. R. Canavin, "The Control of Spacecraft Vibrations Using Multivariable Output Feedback,", American Institute of Aeronautics and Astronautics/American Astronautical Society Astrodynamics Conference, Palo Alto, California, Aug. 7-9, 1978. AIAA Paper 78-1419.

10. L. E. Elliott, D. L. Mingori, and R. P. Iwens, "Performance of Robust Output Feedback Controller for Flexible Spacecraft," Second

VPI&SU/AIAA Symposium on Dynamics and Control of Large Flexible Spacecraft, June, 1979, pp. 409-420.

11. R. L. Forward, "Electronic Damping of Orthogonal Bending Modes in a Cylindrical Mast - Experiment," Journal of Spacecraft, Vol. 18, No. 1, January-February, 1981, pp. 11-17.

12. L. Meirovitch and H. Baruh, "On the Implementation of Modal Filters for Control of Structures," AIAA Guidance and Control Conference, Seattle, August 20-22, 1984. AIAA Paper No. 84-1949.

13. P. C. Hughes, Learning Session on "Control of Flexible Space Structures : Concepts for the Structural Dynamicist," Palm Springs, California, May 19, 1984.

14. J. N. Aubrun, "Theory of the Control of Structures by Low Authority Controllers," Journal of Guidance and Control, Vol. 3, No. 5, September-October, 1984, pp. 444-451.

15. R. B. Preston and J. G. Lin, "Pareto Optimal Vibration Damping of Large Space Structures with Modal Dashpots," Proceedings of the 1980 Joint Automatic Control Conference, Vol. II, Paper FP1-C, August 13-15,1980, (San Francisco).

16. W. L. Brogan, Modern Control Theory, Quantum Publishers, Inc., New Jersey, 1982.

17. W. L. Hallauer Jr. and A. P. Nayak, "Experimental Study of Active Vibration Control," Final Report to the Air Force Office of Scientific Research for Contract F49620-83-C-0158, February, 1985.

18. G. C. Schamel II, "Active Damping of a Structure with Low-Frequency and Closely-Spaced Modes: Experiments and Theory," M. S. Thesis, Virginia Polytechnic Institute and State University, 1985.

19. W. L. Hallauer Jr., G. R. Skidmore, and L. C. Mesquita, "Experimental-Theoretical Study of Active Vibration Control," 1st International Modal Analysis Conference, Orlando, Florida, November 8-10, 1982, Proceedings, pp. 39-45.

20. G. R. Skidmore, W. L. Hallauer Jr., and R. N. Gehling, "Experimental-Theoretical Study of Modal-Space Control," 2nd International Modal Analysis Conference, Orlando, Florida, February 10-12, 1984, Proceedings, pp.66-74.

21. M. A. Masse, "A Plane Grilllage Model for Structural Dynamics Experiments: Design, Theoretical Analysis, and Experimental Testing," M. S. Thesis, Virginia Polytechnic Institute and State University, 1983.

22. R. N. Gehling, "Experimental and Theoretical Analysis of a Plane Grillage Structure with High Modal Density," M. S. Thesis, Virginia Polytechnic Institute and State University, 1984.

23. J. H. Argyris, O. Hilpert, G. A. Malejannakis, and D. W. Scharpf, "On the Geometrical Stiffness of a Beam in Space - a Consistent Approach," Computer Methods in Applied Mechanics and Engineering, Vol. 20, 1979, pp. 105-131.

The vita has been removed from the scanned document